REPUBLIQUE ALGERIENNE DEMOCRATIQUE ET POPULAIRE

MINISTERE DE L'ENSEIGNEMENT SUPERIEUR ET DE LA RECHERCHE SCIENTIFIQUE

FACULTEDE : TECHNOLOGIE
DEPARTEMENT : D'ELECTRONIQE
N°: .....

DOMAINE : SCIENCE ET TECHNOLOGIE
FILIERE : ELECTRONIQUE
OPTION:MICROELECTRONIQUE

ention Du
PAR:

HASNI ABDE ALOUAHAB
HADIDI AYMEN

Intitulé:

THEORETICAL INVESTIGATION OF PHYSICAL PROPERTIES OF SOME DELAFOSSITE COMPOUNDS

Soutenu devant le jury composé de:

HADJAB Moufdi	**Université Mohamed Boudiaf M'sila**	**Président**
KETFI Mohamed El-Amin	**Université Mohamed Boudiaf M'sila**	**Rapporteur**
SAAD ESSAOUD Saber	**Université Mohamed Boudiaf M'sila**	**Examinateur**

Le **24/06/2025**

Année universitaire : 2024 / 2025

بسم الله الرحمن الرحيم

شكرا إلى من له الفضل أولاً وآخراً، ظاهرًا وباطنًا،
إلى الله سبحانه وتعالى، الحمد لله الذي بنعمته تتم الصالحات،
.وهو الذي وفقني ويسر لي سبل العلم والتعلم، وأسأله أن يجعل هذا العمل خالصًا لوجهه الكريم

فهو جدير بالثناء والشكر .. وأقدر جهوده المضنية وتوجيهاته الثمينة ودعمه اللامحدود "كتفي محمد الامين"أتقدم بالشكر لأستاذي الكريم
..التقدير وله مني كل

و أتوجه بجزيل الشكر إلى لجنة الاساتذة

إلى أهلي الأعزاء، أنتم السند الحقيقي والدعم الدائم، لكم مني كل الشكر والامتنان على ما قدمتموه
.من حب وتشجيع

وإلى طاقم الإدارة الكرام، شكرًا لجهودكم الجبارة وإخلاصكم في العمل

أهدي عملي المتواضع.. إلى كل من علمني حرفا أو أفادني بعلم أو أعانني بالنصيحة! ..

عبد الوهاب

إلى من قال الله تعالى فيهما:

(وقل رب ارحمهما كما ربياني صغيرا)

إلى العزيز الذي حملت اسمه فخراً، من بذل جهد السنين من أجل أن أعتلي سُلم النجاح

والدي

إلى من علّمتني الأخلاق قبل الحروف، إلى من احتضنتني بقلبها قبل يديها، التي كانت دعواتها تُمهّد طريقي، ومهدت لي السبل لأصل

والدتي

إلى مُلهمي الثبات وأمان اليأس، إلى من شددت بهم عُضدي فكانوا لي بمثابة النور في العتمة

إخوتي و أصدقائي

إلى من كانو الشمعة التي تنير دروبنا والمعين الذي لا ينضب..... اساتذتي

أيمن

CHAPITER 01

CHAPITER 02

LIST OF TABL

Introduction General

With the global trend towards renewable energy, scientific research—both experimental and theoretical has accelerated toward harnessing one of the most important sources of sustainable energy: solar energy, where light energy is converted into electrical energy using solar panels and photovoltaic systems [1,2].

The basic idea behind the invention of solar panels is based on the possibility of generating electrical energy by exposing certain materials to light rays. Following this discovery, many studies were conducted, including the discovery of the element selenium, which significantly influenced the advancement of this technology and its use in various fields such as computers and satellites. The efficiency of these photovoltaic technologies depends on many factors, perhaps the most important being the nature of the materials they are made from.

One of the main obstacles to the implementation of solar panels as an energy generation technology is their relatively high cost. Inorganic thin-film solar panels are a proven technology that offers significant cost reductions compared to crystalline photovoltaic technology, which currently dominates the market. Among these are Delafossite oxide compounds, which are a family of materials with a unique crystal structure and interesting electronic properties. These materials are composed of transition metals such as copper, nickel, and cobalt, in addition to oxygen and sometimes-other elements. The crystal structure consists of layers of transition metal ions sandwiched between oxide ions, forming a three-dimensional network.

Various methods derived from Density Functional Theory (DFT) help in solving the Schrödinger equation, revealing insights into structural, elastic, and mechanical properties [2].

Perovskite structures, known for their stability and diverse applications, have long captivated scientific interest [3]. The term "perovskite" originated from CaTiO3, discovered in 1839 and named after Russian mineralogist Lev Aleksevich von Perovski [4].

The aim of this study is to enhance our understanding of the structural, electronic, thermodynamic, and thermoelectric properties of the perovskite compound $AgMnS_2$ using the Wien2k computational software. This research is divided into two main chapters. The first chapter provides a theoretical basis for analyzing crystalline systems, based on the principles of quantum

mechanics. It begins with an exploration of the time-independent Schrödinger equation, which describes the behavior of electrons and nuclei within the system. Key approximations such as Born-Oppenheimer, Hartree, Hartree-Fock, and Density Functional Theory (DFT) are explained, with a particular focus on their role in estimating interactions among electrons.

In the study of regular crystal lattices, the time-independent Schrödinger equation is summarized, describing a system composed of a large number of moving and interacting electrons and nuclei. The main approximations adopted to simplify the solution of the Schrödinger equation are then highlighted, such as the Born-Oppenheimer approximation, the Hartree approximation, the Hartree-Fock approximation, and the Density Functional Theory. In addition, the most important approximations used to evaluate electron interaction are presented. The full-potential linearized augmented plane wave method (FP-LAPW) is then explained, followed by a description of the various software tools used to study the properties of interest.

The second chapter addresses the calculation of structural properties using GGA approximations and has determined some structural properties of the $AgMnO_2$ compound such as lattice constant, bulk modulus, and cohesive energy. The Density Functional Theory (DFT) will be used as the main tool of the study. In the first step, we will perform a structural phase stability analysis for potential phases of the compound. The electronic behavior of the compound was studied, where we determined the energy gap value for each phase, in addition to identifying the electronic orbitals contributing to each energy band by studying the density of states curves.

[1] M. A. Green, “Third generation photovoltaics: Advanced solar energy conversion,” Springer, 2006.

[2] [2] J. P. Perdew, K. Burke, and M. Ernzerhof, “Generalized gradient approximation made simple,” Physical Review Letters, vol. 77, no. 18, pp. 3865–3868, 1996. [

[3] 3] N. A. Spaldin, “A beginner’s guide to the modern theory of polarization,” Journal of Solid State Chemistry, vol. 195, pp. 2–10, 2012.

[4] [4] R. D. Shannon, “Revised effective ionic radii and systematic studies of interatomic distances in halides and chalcogenides,” Acta Crystallographica Section A, vol. 32, pp. 751–767, 1976.

I-1 Introduction

The study of Delafossite compounds has garnered significant attention due to their unique physical properties, which make them promising candidates for various technological applications, including transparent conducting oxides, thermoelectric materials, and catalysts. Delafossites, with the general formula ABO_2, where A is a monovalent cation (e.g., Cu, Ag) and B is a trivalent cation (e.g., Al, Ga, In), exhibit a layered structure that leads to anisotropic electronic, optical, and magnetic properties. Understanding these properties at a fundamental level requires a robust theoretical framework that can accurately describe the electronic structure and interactions within these materials [1].

This chapter theoretical foundations necessary for investigating the physical properties of Delafossite compounds. We begin with the Schrödinger equation, which is the cornerstone of quantum mechanics and provides the basis for understanding the behavior of electrons in solids. We then discuss Density Functional Theory (DFT), a powerful computational tool for electronic structure calculations. Following this, we introduce the Full-Potential Linearized Augmented Plane-Wave (FP-LAPW) method, a highly accurate approach for solving the DFT equations in solids. Finally, we provide an overview of the Wien2k software package, which implements the FP-LAPW method and is widely used in materials science research.[1]

I-2 Schrödinger Equation

Schrödinger, an Austrian theoretical physicist, played a key role in advancing the wave theory of matter. His work was shaped by the foundational ideas of early quantum theory, which were pioneered by figures such as Max Planck, Albert Einstein, and Niels Bohr [2].

The description of a material implies knowing its electronic, structural, etc. properties, which reflect the interactions between the particles that constitute it (electrons and nuclei). Classical mechanics failed to provide answers, so quantum mechanics took over. It is essentially based on the resolution of the Schrödinger equation [2].

The Schrödinger equation is the fundamental equation of quantum physics, like Newton's laws in classical physics [03].

In order to obtain interesting quantities such as energy E or the wave function, it is necessary to solve the time-independent Schrödinger equation, which was established by Erwin Schrödinger in 1925 and is written as follows :

$$\boldsymbol{H\psi\left(\vec{R}_I,\vec{r}_i\right) = E\psi\left(\vec{R}_I,\vec{r}_i\right)} \qquad \text{(I.1)}$$

→ $\boldsymbol{\vec{R}_I}$ vector the coordinate of the nucleus (I).

→ $\boldsymbol{\vec{r}_i}$ vector the coordinate of the electron (i).

→ $\boldsymbol{H}$ Hamiltonian operator associated with the system's total kinetic and potential energy.

→ $\boldsymbol{E}$ eigenvalue Energy of the system.

→ $\boldsymbol{\psi}$ wave function that is dependent on the nucleus and electron coordinates.

the Hamiltonian system, which is composed of electrons and nuclei, contains the potential energies (electron-electron, electron-nucleus, and nucleus-nucleus) as well as the kinetic energy of electrons and nuclei, the expression for the system's total Hamiltonian is as follows:

$$\boldsymbol{H = T_e + T_N + V_{e-e} + V_{e-N} + V_{N-N}} \qquad \text{(I.2)}$$

Such as:

- $\boldsymbol{T_e = -\sum_i^N \frac{h^2}{2m} \nabla_i^2}$ …….. is the kinetic energy of the electrons.
- $\boldsymbol{T_N = -\sum_i^{N\alpha} \frac{h^2}{2M} \nabla_A^2}$ ……..…… is the kinetic energy of atoms.
- $\boldsymbol{V_{e-e} = \frac{1}{2}\sum_i^N \sum_{j\neq i}^N \frac{e^2}{|\vec{r_i}-\vec{r_j}|}}$ …….. is the electron-electron interaction potential.
- $\boldsymbol{V_{N-e} = -\sum_i^N \sum_A^{N\alpha} \frac{Z_A e^2}{|\vec{r_i}-\overrightarrow{R_A}|}}$ …... is the nucleus-electron interaction potential.
- $\boldsymbol{V_{N-N} = \frac{1}{2}\sum_A^N \sum_{B\neq A}^{N\alpha} \frac{Z_A Z_B e^2}{|\overrightarrow{R_A}-\overrightarrow{R_B}|}}$ ..... is the nucleus-nucleus interaction potential.

We can write the Hamiltonian in the form:

$$H = \left[-\sum_i^N \frac{h^2}{2m}\nabla_i^2 - \sum_i^{N\alpha} \frac{h^2}{2M}\nabla_A^2 + \frac{1}{2}\sum_i^N \sum_{j\neq i}^N \frac{e^2}{|\vec{r_i}-\vec{r_j}|} - \sum_i^N \sum_A^{N\alpha} \frac{Z_A e^2}{|\vec{r_i}-\overrightarrow{R_A}|} + \frac{1}{2}\sum_A^N \sum_{B\neq A}^{N\alpha} \frac{Z_A Z_B e^2}{|\overrightarrow{R_A}-\overrightarrow{R_B}|}\right] \quad \text{(I.3)}$$

→ m : is the mass of electron i.

→ M : is the mass of the nucleus.

→ $|\vec{r_i} - \vec{r_j}|$:The distance between the two nuclei α and β

→ $|\vec{r_i} - \overrightarrow{R_A}|$: The distance between the nucleus α and the electron i

→ $|\overrightarrow{R_A} - \overrightarrow{R_B}|$: The distance between the two electrons i and j.

→ The indices i = (1,…, N) and A= (1,… $\boldsymbol{N\alpha}$), are thus adopted in order to distinguish electronic quantities from nuclear quantities. The Schrödinger equation can therefore be represented in the form:

$$\mathbf{H = (T_e + T_N + V_{e\text{-}e} + V_{e\text{-}N} + V_{N\text{-}N})\psi(r_1, r_2, \ldots R_1, R_2, \ldots) = E\psi(r_1, r_2, \ldots R_1, R_2, \ldots)} \quad \text{(I.4)}$$

The number of particles interacting in solid state physics is of the order of the Avogadro number This requires a solution of a system of Schrödinger equations containing a number of simultaneous differential equations of the order. Since it is

difficult to solve this system of equations, they are given even in the case of interactions of a small number of particles. This is why the many approaches to solving this equation rely on some fundamental approximations [04].

I-2 The different approximations of the Schrödinger equation

It can be somewhat difficult to solve the Schrödinger equation, particularly for systems with many moving parts and electrons and their intricate interconnections. In most cases, we are unable to find precise solutions due to its complexity. To get close to the correct answer, scientists employ less complex techniques and educated estimates. Some of the primary ways they accomplish that are as follows:

I-2-1 Born-Oppenheimer Approximation

The approximation developed by Born and Oppenheimer in 1927, known as the Born-Oppenheimer approximation, is a cornerstone in understanding many-body quantum systems, particularly in molecules and crystalline solids.

This approximation relies on the fact that electrons, which are much lighter than nuclei, move significantly faster. Due to this large difference in mass and speed, the motion of electrons can be decoupled from that of the nuclei, greatly simplifying the problem. The kinetic energy of the nuclei is neglected, and the nucleus-nucleus repulsion potential is treated as a constant, reducing the total Hamiltonian to what is known as the electronic Hamiltonian He. The total Hamiltonian of a system of electrons and nuclei (I.2) Under the Born-Oppenheimer approximation, the nuclear kinetic energy term T_N is neglected (since nuclei are assumed to be stationary), and the nucleus-nucleus

potential $V_{N\text{-}N}$ is treated as a constant. This simplifies the Hamiltonian to the electronic Hamiltonian He:

$$\boldsymbol{He} = \boldsymbol{T_e} + \boldsymbol{V_{e-e}} + \boldsymbol{V_{e-N}} \quad \text{(I.5)}$$

Schrödinger equation :

$$\mathrm{H} = (\mathrm{T_e} + \mathrm{V_{e\text{-}e}} + \mathrm{V_{e\text{-}N}})\Psi_e(\overrightarrow{R_I} - \overrightarrow{r_i}) = \mathrm{E}_e(\overrightarrow{R_I})\Psi_e(\overrightarrow{R_I} - \overrightarrow{r_i}) \quad \text{(I. 6)}$$

This Hamiltonian focuses solely on the motion of electrons in the presence of fixed nuclei, making the solution of the quantum equations for electrons more tractable. Subsequently, the motion of the nuclei can be studied separately on a potential energy surface generated by the electron distribution. This approximation is a fundamental tool in quantum chemistry and solid-state physics, contributing to the understanding of electronic, optical, and thermal properties of materials.

Although this approximation leads to large simplifications when solving the Schrödinger equation for molecules [17] and the Hamiltonian becomes simpler, it remains insufficient due to the interactions between electrons which are very complicated, thus forced us to resort to additional simplifications such as the Hartree and Hartree-Fock approximations [14]

I-2-2 The Hartree Approximation

This approximation was first developed by Douglas Hartree in 1928 [07]. It is an approach that assumes each electron moves independently in the mean field created by the other electrons and the nuclei. So, the problem shifts from a system of electron-electron pair repulsion to a problem of a particle immersed in an average electrostatic field created by the charge distribution of all the other electrons and nuclei. This approximation reduces the problem from N interacting bodies to that of independent electrons, which allows for the description of the wave function of the electronic system. $\boldsymbol{\psi}(\boldsymbol{r}_1, \boldsymbol{r}_2, \ldots, \boldsymbol{r}_N)$ becomes like the direct product of the single-electron wave functions $\boldsymbol{\psi_i}(\boldsymbol{r}_i)$ [05].

$$\boldsymbol{\psi}(\boldsymbol{r}_1, \boldsymbol{r}_2, \ldots, \boldsymbol{r}_N) = \boldsymbol{\psi}(\boldsymbol{r}_1).\boldsymbol{\psi}(\boldsymbol{r}_2) \ldots\ldots \boldsymbol{\psi}(\boldsymbol{r}_N) \quad (\text{I}.7)$$

The Hamiltonian is written as a sum of Hamiltonians, each describing the behavior of a single electron:

$$H = \sum_i h_i \quad (\text{I}.8)$$

With:

$$h_i = \frac{h^2}{2m}\nabla_i^2 + V_{ext} + V_i^H \quad (\text{I}.9)$$

$\frac{h^2}{2m}\nabla_i^2$: Kinetic energy of the electron.

V_{ext} : represents both the potential due to the nuclei.

V_i^H : is the Hartree potential for the electron.

The Hartree potential for the electron replaces the electrostatic electron-electron interaction with all other electrons, and it is given by the following relation [03]:

$$V^H = \int d^3 r \frac{\rho(r')}{|r-r'|'} \quad (\text{I}.10)$$

The electron density in equation (I.10) is given by:

$$\rho_i = \sum_{j(j\neq i)}^{N} \left|\boldsymbol{\psi}_j(\vec{r})\right|^2 \quad (\text{I}.11)$$

The potential that the electron experiences in the field of all the α nuclei is (the electron-nuclei interaction) is V_{ext}

$$V_{ext}(\vec{r}) = -Ze^2 \sum_R \frac{1}{|\vec{r}-R|} \quad (\text{I}.12)$$

We express the effective potential as the sum of these two contributions:

$$V_{eff}(\vec{r}) = V^{H}(\vec{r}) + V_{ext}(\vec{r}) \quad (\text{I. } 13)$$

Nevertheless, this approximation suffers from various problems: The main flaw of the Hartree method is that it does not take into account the Pauli principle. This method treats electrons as distinguishable particles and neglects electronic correlation and exchange effects. This necessitates the use of other approaches to better describe the term responsible for this contribution [06].

I-2-3 The Hartree – Fock Approximation

The Hartree-Fock method is widely used in atomic physics and condensed matter physics, where it provides an approximate solution to the Schrödinger equation for a system of multiple particles. Hartree-Fock is a method for exploring the role of electronic correlations, based on the variational principle which specifies that the ground state energy of the given system calculated as the expected value of the proposed wave function is always greater than, or equal to, the energy that is the exact solution of the Schrödinger equation. The studied system of N electrons can be described by the wave function ψ^{HF} composed of the spinorbitals $\psi_i(x)_i$ of N in the form of the Slater determinant [07]:

$$\psi^{HF}(x_1, x_2, \dots, x_N) = \frac{1}{\sqrt{N!}} \begin{vmatrix} \varphi_1(x_1) & \varphi_2(x_1) & \dots & \varphi_N(x_1) \\ \varphi_1(x_2) & \varphi_2(x_2) & \dots & \varphi_N(x_2) \\ \vdots & \vdots & \ddots & \vdots \\ \varphi_1(x_N) & \varphi_2(x_N) & \dots & \varphi_N(x_N) \end{vmatrix} \quad (\text{I. } 14)$$

Where $\frac{1}{|\sqrt{N}|}$: is the normalization factor

Spin orbitals $\psi_i(x)_i$ are the solutions of the Hartree-Fock equation:

$$F\varphi_i(x_i) = \varepsilon_i \varphi_i(x_i) \quad (\text{I. } 15)$$

Where F is the Hartree-Fock operator defined for an electron by

$$F = -\frac{\hbar^2}{2m}\nabla_i^2 + V_{ext} + V^{HF} \quad (\text{I}.16)$$

V^{HF}: is the Hartree-Fock potential that represents the potential applied to electron i by the other electrons. This potential is expressed using two operators J and K [09].

$$V^{HF} = \sum_i J_i(x_i) - K_i(x_i) V^{HF} = \sum_i J_i(x_i) - K_i(x_i) \quad (\text{I}.17)$$

With:

$$J_i(x_1)\left|\varphi_j(x_1)\right\rangle = \left(\int \varphi_i^*(x_2)\frac{1}{|\overrightarrow{r_2}-\overrightarrow{r_1}|}\varphi_i(x_2)dx_2\right)\left|\varphi_j(x_1)\right\rangle \quad (\text{I}.18)$$

$$K_i(x_1)\left|\varphi_j(x_1)\right\rangle = \left(\int \varphi_i^*(x_2)\frac{1}{|\overrightarrow{r_2}-\overrightarrow{r_1}|}\varphi_j(x_2)dx_2\right)\left|\varphi_i(x_1)\right\rangle \quad (\text{I}.19)$$

Where:

$j_i(x_1)$: is the Coulomb operator.

$K_i(x_1)$: is the exchange operator.

This method neglects any correlation between the relative positions of two electrons other than that introduced by the antisymmetric form. It can therefore only handle systems with few electrons, such as small molecules. The Hartree-Fock method remains, nonetheless, an indispensable benchmark [07].

I-3 Density Functional Theory (DFT)

Density Functional Theory (DFT) was originally developed primarily within the framework of non-relativistic quantum theory and the Born-Oppenheimer approximation [10]. The Schrödinger equation $H\psi = E\psi$ and Quantum mechanics provide the ideal framework for describing the N electron wave function of the

studied system $\psi(\boldsymbol{r}_1, \boldsymbol{r}_2, \ldots, \boldsymbol{r}_N)$ [11]. Hence, the N_e electrons are replaced by the total electronic density which depends only on 3 spatial variables. Historically, the first ideas in this direction were introduced in the works of Thomas and Fermi in 1927. In their model, electronic interactions are treated classically and the kinetic energy is calculated based on a homogeneous electronic density. However, it should be noted that DFT was actually established with the exact fundamental theorems of Hohenberg [12] and Kohn in 1964 [10], which uniquely relate the ground state energy and its density.

The development of new methods in quantum mechanics, such as Density Functional Theory (DFT), was driven by the limitations of earlier approaches like the Hartree-Fock (HF) method. The HF method, while foundational, has significant drawbacks: it relies on wavefunctions as the primary variable, leading to computationally expensive calculations due to the large number of variables involved. Moreover, the resulting wavefunctions often lack direct physical meaning, and the method fails to account for electron correlation effects, which are crucial for accurately describing many physical and chemical systems. These limitations made HF impractical for studying complex materials, molecules, and systems where electron interactions play a dominant role [13].

Methode HF	**Methode DFT**
	

Figure I .1: methods of Hartree-Fock and the Density Functional Theory (DFT)

To address these challenges, DFT emerged as a more efficient and versatile alternative. By using electron density as the fundamental variable, DFT significantly reduces the computational complexity and allows for the study of larger systems. Grounded in the Hohenberg-Kohn theorems, DFT transforms the many-body problem into a more manageable form through the Kohn-Sham equations. Crucially, DFT incorporates electron correlation effects via the exchange-correlation functional, enabling more accurate predictions of electronic, structural, and chemical properties. This combination of computational efficiency and improved accuracy has made DFT indispensable in fields like materials science, chemistry, and nanotechnology, where understanding the behavior of electrons in complex systems is essential. Thus, the need for new methods like DFT arose from the demand for more practical, accurate, and scalable tools to tackle the limitations of traditional approaches like HF [14].

I-3-1 Formulation of Density Functional Theory (DFT)

The basis of Density Functional Theory (DFT) is to write the total energy of a system containing multiple interacting electrons as a function of the electron density, that is, the calculation of the system's energy based on the electron density instead of its wave function, where the expression for the electron density is given by the formula [15]:

$$\rho(\vec{r}) = \sum_{i=1}^{N} |\Psi_i(\vec{r})|^2 \qquad (\mathrm{I}.20)$$

Density Functional Theory (DFT) is based on two main axes:

I-3-1-1 Theorems of Hohenberg and Kohn

The two theorems presented by Hohenberg and Kohn in 1964, [25–27] are considered the foundation of density functional theory, these two theorems are proven in the articles [28–31].

A- First theorem:

For any system of interacting particles in an external potential $V_{ext}(r)$, the potential is determined when the particle density $p(r)$is in its ground state. The total energy E is written in the form [16]

$$E(\rho) = F(\rho) + \int_{\rho} \rho\,(r) V_{ext}(r) d^3r \qquad (I.21)$$

Where :

$$F[(\rho)] = T[(\rho)] + V_{e-e}[(\rho)] \qquad (I.22)$$

With:

→ $F[(\rho)]$: is a universal function of the electronic density.

→ T : Kinetic energy.

→ V_{e-e} :The energy of electron-electron interaction.

B -Second theorem:

This theorem states that the energy of a non-degenerate ground state can be determined by the density that minimizes the energy of the ground state. we have [15]:

$$E_0 \leq E(\rho) \quad (I.23)$$

Thus, to obtain the energy of the ground state, we will seek to minimize the total energy functional of the system by applying the variational principle (minimization of the energy functional). Then we write the minimization relation as follows [14]:

$$\frac{dE[\rho(r)]}{d\rho(r)} = 0 \quad (I.24)$$

We find:

$\frac{dF[\rho(r)]}{d\rho(r)} + \mathrm{V_{ext}}(r) = 0 \quad (\mathrm{I}.25)$

In this expression, the formulas for kinetic energy and exchange-correlation remain unknown, with all the properties of a system defined by an external potential $\mathrm{V_{ext}}$can be determined from the electronic density of the ground state. The energy of the system $\mathrm{E}(\rho)$reaches its minimum value if the electronic density is that of the ground state.

There remains a significant problem to solve how to rewrite an exact analytical formulation of the functional $F[(\rho)]$ for a system with N interacting electrons.

I-3-1-2 The Kohn-Sham equation

Kohn and Sham (KS) used variational properties to determine the ground state energy and obtain a description of the functional. The idea of Kohn-Sham is to introduce a system of non-interacting particles whose ground state is characterized at every point by the same density $p(\mathrm{r})$ as that of the real ground state. This implies independent particle equations for the non-interacting system, grouping all the complicated and difficult-to-evaluate terms into an exchange-correlation functional [17].

$$E_{KS}[\rho(r)] = F[\rho(r)] + \int V_{ext}(r)\rho(r)d^3r \qquad (\mathrm{I}.26)$$

$$= T_s[\rho(r)] + E_H[\rho(r)] + E_{xc}[\rho(r)] + \int V_{ext}(r)\,\rho(r)d^3r$$

Where:

→ Ts The kinetic energy of the non-interacting electron gas.

→ $E_{xc}[\rho(r)]$: Is an additional functional that describes the inter-electronic interaction called exchange-correlation energy.

→ $V_{ext}(r)$Includes the Coulomb interaction with the nuclei and that of the nuclei with each other.

With:

$$E_H[\rho(r)] = \frac{1}{2}\int d^3r d^3r' \frac{\rho(r)\rho(r')}{|r-r'|} \qquad (I.27)$$

The wave functions of a single particle are the N solutions of the lowest energy. of the Kohn-Sham equation. $(H_{KS} - \varepsilon_i)\psi_i(r) = 0$

ε_i: The eigenvalue.

H_{KS}: The effective Hamiltonian.

$$H_{KS} = -\frac{\hbar^2}{2m}\Delta_i + V_{KS} \qquad (I.28)$$

$$V_{KS}(r) = V_{ext}(r) + V_H[\rho] + V_{xc}[\rho] \qquad (I.29)$$

V_H: The Hartree potential given by:

$$V_H = \int \frac{\rho(r')}{|r-r'|} dr' \qquad (I.31)$$

V_{xc}: The potential for exchange and correlation given by

$$V_{xc} = V_x + V_c \qquad (I.31)$$

The exchange-correlation potential is obtained from the derivative of the energy. With respect to the density:

$$V_{xc}(\vec{r}) = \frac{\partial E_{xc}[\rho(\vec{r})]}{\partial \rho(\vec{r})} \qquad (I.32)$$

$$H_{KS}\psi_i(\vec{r}) = \varepsilon_i\psi_i(\vec{r}) \qquad (I.33)$$

$$\left[-\frac{\hbar^2}{2m}\Delta_i + V_{eff}(\vec{r})\right]\psi_i(\vec{r}) = \varepsilon_i\psi_i(\vec{r}) \qquad (I.34)$$

Solving the Kohn-Sham equation depends on two basic steps:

- The first step: define all the terms of the effective Kohn-Sham potential, i.e. the exchange correlation potential E_{xc} must be determined because this term has no mathematical formula but it can be estimated by approximations.

- The second step: find the wave functions (Kohn-Sham orbits), which represent a solutions for the Kohn-Sham equation given by [3]:

$$\varphi_{KS}(\vec{r}) = \sum_j C_{ij}\ \varphi_j(\vec{r}) \qquad (I.35)$$

Where $\varphi_i\ (\vec{r})$ are the basis functions and C_{ij} are the development coefficients.

$$\sum_j C_{ij}\ H_{KS}\Big|\varphi_j| = \sum_j C_{ij}\ \varepsilon_{KS}|\varphi_j| \qquad (I.36)$$

$$\langle\varphi_k|\textstyle\sum_j C_{ij}\ H_{KS}|\varphi_j\rangle = \langle\varphi_k|\sum_j C_{ij}\ \varepsilon_{KS}|\varphi_j\rangle \qquad (I.37)$$

$$\textstyle\sum_j \quad \big(\langle\varphi_k|H_{KS}|\varphi_j\rangle - \varepsilon_{KS}\langle\varphi_k|\varphi_j\rangle\big)C_{ij} = 0 \qquad (I.38)$$

It remains to determine the coefficients C_{ij} by inserting a developed basis into the Kohn-Sham equation. The Kohn-Sham equation is solved using an iterative loop illustrated in figure (I.2), where the process is started using an initial density P_{in} for the first iteration, this density is used to P_{in} solve the Kohn-Sham equation, then, We use a superposition of atomic densities, then we calculate the Kohn-Sham matrix, and we solve the equations for the expansion coefficients to obtain the Kohn-Sham orbitals.

After this step, by calculating the new density P_{out}, we perform a test (if the density or energy has changed significantly, we return to the first step; otherwise, we mix the two charge densities P_{out} and P_{in} as follows [3]:

$$\rho_{in}^{i+1} = (1-\alpha)\rho_{in}^{i} + \rho_{out}^{i} \qquad (I.39)$$

Thus, the iterative procedure can be repeated until the convergence condition is met [3].

A Self-consistent calculation is an iterative process used in computational methods like Density Functional Theory (DFT) and Hartree-Fock (HF) to solve the electronic structure of a system. It begins with an initial guess for the electron density or wavefunctions, which is used to construct an effective potential. The Kohn-Sham (for DFT) or Hartree-Fock equations are then solved to obtain new orbitals and eigenvalues. Using these orbitals, the electron density is updated and compared to the previous density. If the change is below a predefined threshold, the calculation is considered converged, and the final results (e.g., total energy, electron density, and orbitals) are output. If not, the process repeats with the updated density until convergence is achieved. This iterative approach ensures that the solution is consistent with the system's physical properties.

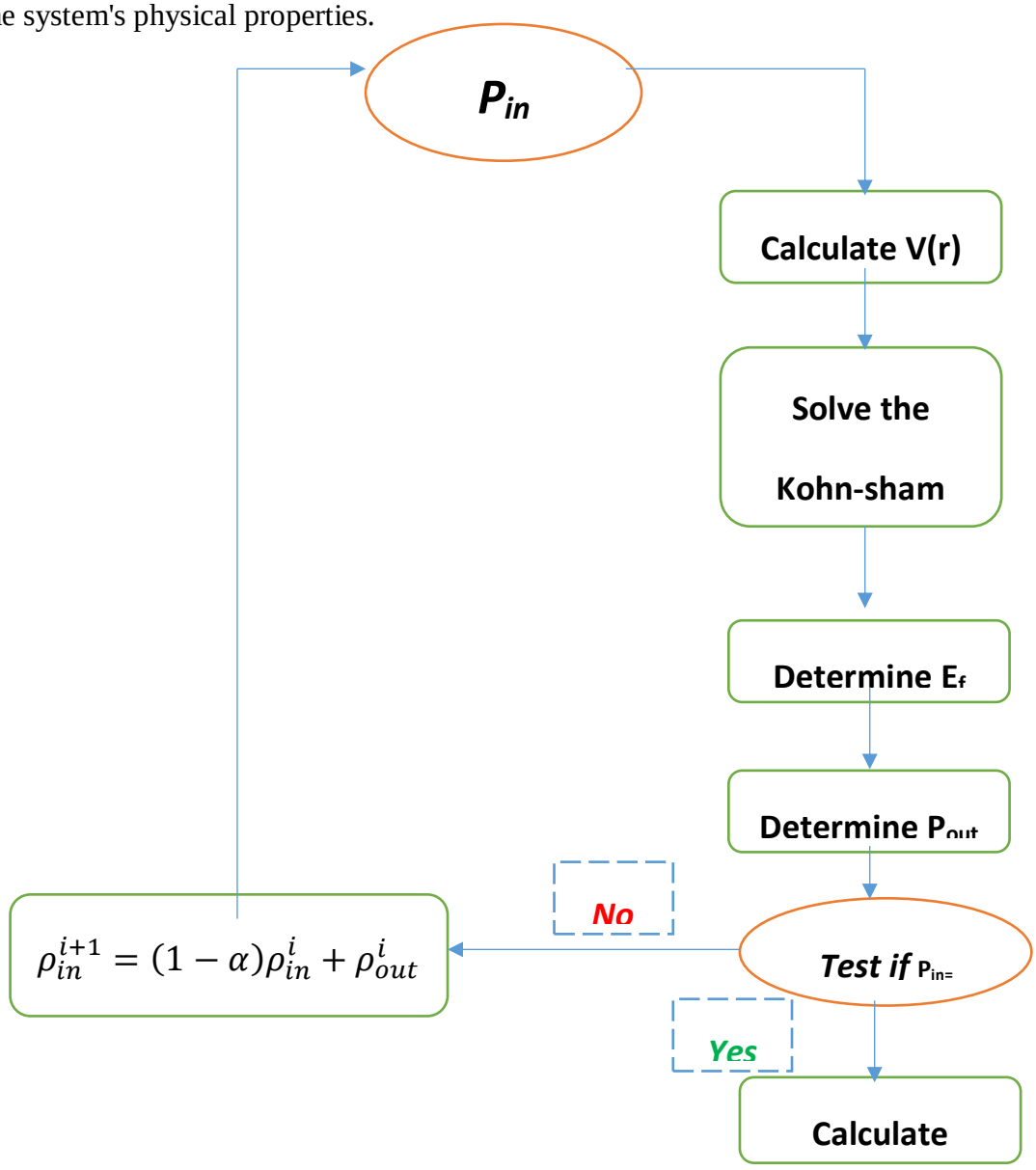

Figure I. 2: Self-consistent calculation flowchart.

I- 4 The Different Types of Approximation of the $E_{xc}[\rho]$

The exchange-correlation potential between electrons lacks an analytical expression, hence many methods have been used to estimate its values. The mathematical formulation selected for this potential largely determines the accuracy of the results produced [18].

I- 4-1 Local density approximation (LDA/LSDA):

The LDA approximates the exchange-correlation energy E_{xc} of an inhomogeneous electron system (e.g., atoms, molecules, or solids) by assuming that the exchange-correlation energy at each point in space depends only on the local electron density $\rho(\vec{r})$ at that point. Mathematically, the exchange-correlation energy in LDA is expressed as:

$$E_{XC}^{LSDA} = \int \rho(\vec{r}) E_{xc}[\rho(\vec{r})] d\vec{r} \qquad (I.40)$$

$$V_{xc} = \frac{dE_{XC}^{LDA}[\rho]}{d\rho} = \varepsilon_{XC}^{LDA} + \rho(\vec{r}) \frac{d\varepsilon_{XC}^{LDA}}{d\rho} \qquad (I.41)$$

→ $\rho(\vec{r})$ is the electron density at position r.

→ $E_{xc}(n(r))$ is the exchange-correlation energy per particle of a uniform electron gas with density $\rho(\vec{r})$.

For each spin up or down magnetic order, the total electron density becomes the sum of the two electron densities

$$\rho(\vec{r}) = \rho_{\uparrow}(\vec{r}) + \rho_{\downarrow}(\vec{r}) \qquad (I.42)$$

The Kohn-Sham equation for the two spins in the form [3]:

$$\begin{cases} \left(\frac{-\hbar^2}{2m}\nabla^2 + V_{eff}^{\dagger}(\vec{r})\right)\varphi_i(\vec{r}) = \varepsilon_{KS}^{\dagger}\varphi_i(\vec{r}) \\ \left(\frac{-\hbar^2}{2m}\nabla^2 + V_{eff}^{\dagger}(\vec{r})\right)\varphi_i(\vec{r}) = \varepsilon_{KS}^{\dagger}\varphi_i(\vec{r}) \end{cases} \qquad (I.43)$$

The Local Density Approximation (LDA) and its spin-polarized extension (LSDA) are foundational approximations in DFT that provide a simple and efficient way to estimate the

exchange-correlation energy. While they have limitations, they remain important tools for studying a wide range of materials and systems [19].

I- 4-2 The Generalized Gradient Approximation GGA

The Generalized Gradient Approximation (GGA) is an improvement over the Local Density Approximation (LDA) in Density Functional Theory (DFT) [20]. It is used to describe the exchange-correlation energy of an electronic system more accurately than LDA by considering not only the local electron density n(r), but also its gradient ∇ n(r). Here is a detailed explanation:

$$E_{xc}^{GGA}[\rho(r)] = \int f[\rho(r), |\nabla\rho(r)|]dr \qquad (I.44)$$

→ $\nabla\rho(r)$ is the gradient of the electron density, which describes how the density varies in space.

The Generalized Gradient Approximation (GGA) improves upon the Local Density Approximation (LDA) by incorporating information about the spatial variation of electron density through its gradient, enabling a more accurate description of systems with rapidly changing electron densities, such as atoms, molecules, and surfaces. GGA addresses key limitations of LDA, including better prediction of molecular binding energies, improved estimation of electronic band gaps (though gaps are still often underestimated), and more accurate descriptions of structural properties and cohesive energies of materials. Additionally, GGA's flexibility makes it adaptable to a wide range of systems, from molecules and solids to surfaces and interfaces, making it a versatile and widely used method in electronic structure calculations [21].

Both LDA (Local Density Approximation) and GGA (Generalized Gradient Approximation) in density functional theory (DFT) are powerful tools for studying the electronic properties of materials, but they have notable limitations. A key issue is their tendency to underestimate band gaps in semiconductors and insulators, as they fail to fully account for non-local exchange-correlation effects. Additionally, these methods struggle to accurately describe strongly correlated systems, such as transition metal oxides, where electron-electron interactions play a critical role. Furthermore, the accuracy of GGA results heavily depends on the choice of functional, and there is no universal functional that works well for all types of systems. These limitations highlight the need for more advanced methods, such as hybrid functionals or DFT+U, to address these shortcomings [22].

I-5 Full-Potential Linearized Augmented Plane-wave Method FP-LAPW

The augmented plane wave method with linearization (FP-LAPW) The FP-LAPW method is primarily the LAPW (Linearized Augmented Plane Wave) method used with a full potential resulting from an improved modification of the so-called augmented plane wave (APW) method developed by Slater. Thus, before delving into the description of the FPLAPW method, we must review some aspects related to the APW method [23].

I-5-1 The augmented plane wave (APW) method

In 1937, Slater presented the APW method in his article. The APW method is the most popular technique for solving the electronic structure using the Kohn-Sham equations, In the vicinity of an atomic nucleus, the potential and wave functions are of the "Muffin-Tin" (MT) form, exhibiting spherical symmetry within the MT sphere of radius. Between the atoms, the potential and wave functions can be considered smooth. Consequently, the wave functions of the crystal are developed in different bases depending on the region considered: Radial solutions of the Schrödinger equation inside the MT sphere and plane waves in the interstitial region [24].

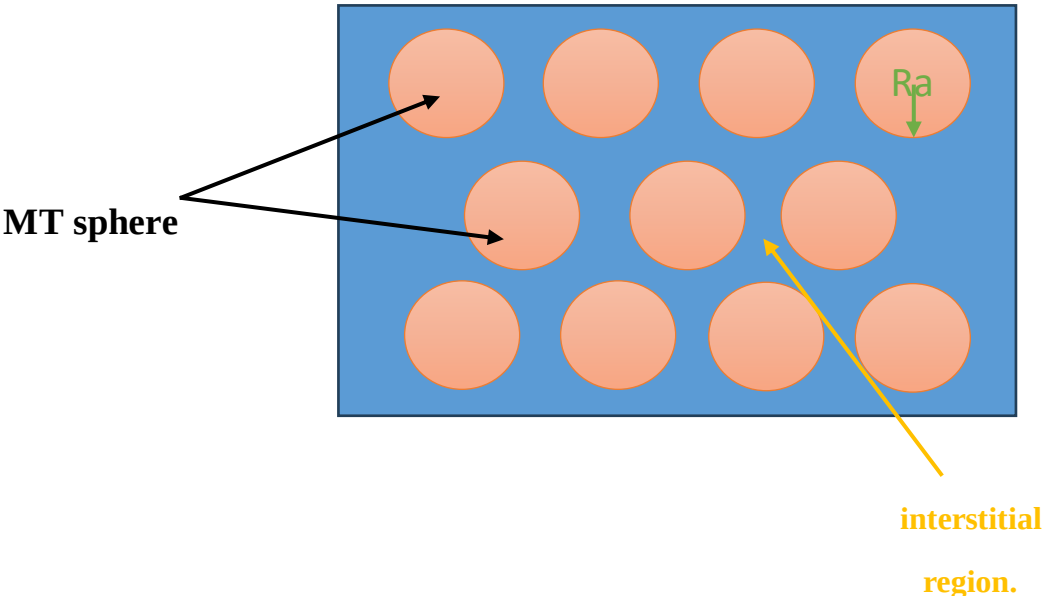

Figure I.3: Diagram of the distribution of the unit cell in atomic spheres and interstitial region.

According to the Slater approximation, the core electrons located inside the sphere are subjected to the spherical potential, whereas in the interstitial region the potential is constant. So, the potential in both regions is given in the form:

$$V(\bar{\bar{r}}) = \begin{cases} v(r) & r \leq R_\alpha \\ 0 & r \geq R_\alpha \end{cases} \qquad (\text{I}.45)$$

Moreover, the waves that describe the behavior of electrons inside the MT spheres differ from those in the interstitial region; they are described by plane waves in the interstitial region, while inside the spheres, they are described by radial functions multiplied by spherical harmonics. The two different wave functions are given by the following expression:

$$\varphi(\vec{r}) = \begin{cases} \sum_{l=0}^{\infty} \sum_{l=0}^{m} A_{lm}\, U_l(r) Y_{lm}(r) & r \leq R_\alpha \\ \frac{1}{\sqrt{\Omega}} \sum_G C_G\ e^{i(\vec{K}+\vec{G})\vec{r}} & r > R_\alpha \end{cases} \qquad (\text{I}.46)$$

Where

→ Ω The cell volume

→ Y_{im}: The spherical harmonics

→ A_{im}: The coefficients of the expansion

→ C_G , A_{im} the coefficients of the expansion in spherical harmonics. The function is a regular solution of the Schrödinger equation for the radial part, which is written in the form[41]:

$$\left[-\frac{d^2}{dr^2}+\frac{l(l+1)}{r^2}+V(r)-E_l\right]ru_l(r)=0 \qquad (\text{I}.47)$$

→ $V(r)$: represents the muffin potential -tin

→ E_l : represents the linearization energy

This equation defines the radial function orthogonal to any eigenstate of the same Hamiltonian that vanishes at the boundary of the spheres. The overlap of the latter is constructed from:

$$(E_2-E_1)ru_1u_2=u_2\frac{d^2u_1}{dr^2}-u_1\frac{d^2u_2}{dr^2} \qquad (\text{I}.48)$$

Where $\boldsymbol{u_1}$ and $\boldsymbol{u_2}$ are the radial solutions to the different energies $\boldsymbol{E_1}$ and $\boldsymbol{E_2}$ respectively.

Slater introduces a modification to this particular choice of these functions by noting that plane waves are solutions to the Schrödinger equation when $\boldsymbol{E_1}$ the potential is constant. As for the radial functions, they are solutions in the case of a spherical potential, when is an eigenvalue.

This approximation is very good for materials with a face-centered cubic structure, and increasingly less satisfactory as the material's symmetry decreases.

To ensure the continuity of the function $\boldsymbol{\phi(r)}$at the surface of the **MT** sphere, the coefficients A_{im} must be developed in terms of the coefficients $\boldsymbol{C_G}$ of the plane waves existing in the interstitial regions. Thus, after some algebraic calculations, we find that:

$$A_{lm} = \frac{4\pi i^l}{\sqrt{\Omega}\, u_l(R_\alpha)} \sum_G C_G \; J_l(|k+g|R_\alpha) y^*_{lm}(k+G) \qquad \text{(I. 49)}$$

The origin is taken at the center of the sphere, and the coefficients A_{im} are determined from those of the plane waves $\boldsymbol{C_G}$. The parameters of the eigenenergy $\boldsymbol{E_l}$ are called the variational coefficients of the APW method. The individual functions, labeled by G, thus become compatible with the radial functions in the spheres, and we then obtain augmented plane waves (APWs).

The APW functions are solutions to the Schrödinger equation in spheres, but only for the energy $\boldsymbol{E_l}$. Consequently, the energy $\boldsymbol{E_l}$ must be equal to that of the G - index band. This means that the energy bands (for a k-point) cannot be obtained by simple diagonalization, and that it is necessary to treat the secular determinant as a function of energy.

The APW method, as constructed, presents some difficulties related to the function $\boldsymbol{U_l(R_\alpha)}$ that appears in the denominator of the equation. Indeed, depending on the value of the parameter $\boldsymbol{E_l}$, the value of $\boldsymbol{U_l(R_\alpha)}$ can become zero at the surface of the MT sphere, leading to a separation of radial functions from plane wave functions. In order to overcome this problem, several modifications to the APW method have been made, notably those proposed by Koelling and Andersen. The modification consists of representing the wave function $\boldsymbol{\phi(r)}$inside the spheres as a linear combination of the radial functions U_l(r) and their derivatives with respect to energy $\dot{U}$(r), thus giving rise to the FP-LAPW method [25].

I-5-2 Principle of the method FP-LAPW

In the FP-LAPW method, the basis functions in the MT spheres are linear combinations of the radial functions $E_l(r), Ylm(r)$à and their derivatives $\dot{E}_l(r), Ylm(r)$with respect to energy. The functions U_l are defined as in the APW method and the function$E_l(r), Ylm(r)$ must satisfy the following condition [26]:

$$\left\{-\frac{d^2}{dr^2}+\frac{l(l+1)}{r^2}+V(r)-E_i\right\}r\dot{U}_l(r)=rU_l(r) \qquad (\mathrm{I}.50)$$

In the non-relativistic case, these radial functions U_l and $\dot{U}l$ ensure, at the surface of the MT sphere, continuity with the plane waves from the outside. Then, the functions wavefunctions thus augmented become the basis functions (LAPW s) of the FPLAPW method:

$$\varphi(r)=\begin{cases}\frac{1}{\sqrt{\Omega}}\sum_G C_G\ e^{i(\vec{K}+\vec{G})\vec{r}} & r>R_\alpha \\ \sum_{lm}^{\infty}[A_{lm}U_l(r)+B_{lm}U_l(r)]Y_{lm} & r<R_\alpha\end{cases} \qquad (\mathrm{I}.51)$$

Where the coefficients B_{lm} correspond to the function U_l and are of the same nature as the coefficients A_{lm} The LAPW functions are plane waves only in the interstitial regions, as in the APW method. Inside the spheres, LAPW functions are better suited than APW functions. Indeed, if E_l differs slightly from the band energy E, a linear combination will better reproduce the radial function than the APW functions.

Therefore, the function U_l can be developed in terms of its derivative U_l and the energy E_l .

$$U_l(E,r)=U_l(E_l,r)+(E-E_l)\dot{U}_l(E,r)+O[(E-E_l)^2] \qquad (\mathrm{I}.51)$$

The FP-LAPW (Full-Potential Linearized Augmented Plane Wave) method ensures the continuity of the wave function at the surface of the Muffin-Tin (MT) sphere. However, this approach comes at the cost of reduced precision compared to the APW (Augmented Plane Wave) method, which reproduces wave functions more accurately. Specifically, the FP-LAPW method introduces an error in the wave functions on the order of $\Delta\psi$ and an error in the band energies on the order of ΔE.

Despite these errors, the LAPW basis functions provide a robust framework that allows, with a single k-point, to obtain all valence bands across a wide energy range. When this is not feasible, the energy window can typically be divided into two parts, which is a significant simplification compared to the APW method.

if the wave function ψ is zero at the surface of the MT sphere, its derivative ψ' will be non-zero. As a result, the issue of continuity at the MT sphere surface does not arise in the FL-LAPW (Full-Potential LAPW) method. This makes FL-LAPW a practical and efficient approach for electronic structure calculations, despite its slight loss in precision compared to APW.

I-5-3 The roles of linearization energies

The linearization energies play a crucial role in electronic structure calculation methods based on Linearized Augmented Plane Waves (LAPW), such as the FP-LAPW (Full-Potential Linearized Augmented Plane Wave) method. Here are their main roles [27]:

1. Linearization of Radial Equations:

- The linearization energies (usually denoted as E_l) are used to linearize the radial solutions of the Schrödinger equation inside the MT (Muffin-Tin) spheres.
- This linearization simplifies calculations by avoiding the direct solution of radial differential equations for each energy, making the LAPW method more numerically efficient.

2. Construction of Basis Functions:

- The linearization energies determine the points around which the radial solutions (basis functions) are expanded in a Taylor series.
- These basis functions are then used to describe electronic states inside the MT spheres, while being coupled to plane waves in the interstitial region.

3. Accuracy of Calculations:

- The choice of linearization energies affects the accuracy of the results. They must be chosen close to the energies of the electronic states of interest (e.g., valence or core states).

- If the linearization energies are poorly chosen, it can lead to errors in the wavefunctions and band energies.

4. Flexibility in Describing Electronic States:

- Linearization energies allow for the description of both valence states (usually near the Fermi level) and core states (more deeply bound).
- To improve accuracy, multiple linearization energies can be used for different groups of states (e.g., one for valence states and another for core states).

5. Simplification of Calculations Compared to APW:

- Unlike the APW (Augmented Plane Wave) method, which requires solving radial equations for each energy, the LAPW method uses linearization energies to avoid this computationally expensive step.
- This makes the LAPW method faster and more practical for electronic structure calculations, while maintaining good accuracy.

6. Continuity of Wavefunctions:

- Linearization energies help ensure the continuity of wavefunctions and their derivatives at the surface of the MT spheres, which is essential for the physical consistency of the results.

linearization energies are key parameters in the FP-LAPW method that simplify calculations while maintaining an accurate description of electronic states. Their careful selection is essential for obtaining reliable and precise results [15].

I-6 Code WIEN2k

WIEN2k is a highly advanced computational software package designed for electronic structure calculations of solids, based on Density Functional Theory (DFT). It utilizes the Full-Potential Linearized Augmented Plane Wave (FP-LAPW) method,

which is recognized as one of the most accurate approaches for investigating the electronic, optical, magnetic, and structural properties of materials[27].

Developed by a team of researchers at the Vienna University of Technology, WIEN2k has become an indispensable tool in the fields of condensed matter physics, materials science, and chemistry.

Its ability to provide precise and reliable results has made it a favorite among researchers worldwide.

I-6 -1 Key Features of WIEN2k

WIEN2k is distinguished by its precision and versatility. Some of its standout features include [28]:

- Full-Potential Approach: Unlike pseudopotential methods, WIEN2k treats the potential without approximations, ensuring high accuracy in calculations.
- FP-LAPW Method: This method divides the unit cell into Muffin-Tin (MT) spheres and an interstitial region, allowing for an accurate description of both localized and delocalized electronic states.
- Wide Range of Applications: WIEN2k can calculate properties such as band structures, density of states (DOS), charge densities, optical properties, magnetic properties, and more.
- User-Friendly Interface: While primarily command-line driven, WIEN2k provides graphical tools for visualization and analysis, making it accessible to both beginners and advanced users.

I-6-2 Methodology and Theoretical Background

The WIEN2k software is based on the FP-LAPW method, which is a realization of DFT. The key steps in its methodology include [29]:

- Division of Space: The unit cell is divided into non-overlapping MT spheres (around atomic sites) and an interstitial region.

- Basis Functions: Inside the MT spheres, the wavefunctions are expanded in terms of spherical harmonics and radial functions, while plane waves are used in the interstitial region.
- Linearization Energies: These are used to linearize the radial Schrödinger equation, improving computational efficiency.
- Self-Consistent Calculations: WIEN2k solves the Kohn-Sham equations iteratively until self-consistency is achieved in the electron density and potential[33].

I-6-3 Applications of WIEN2k

WIEN2k has been used extensively in research to study a wide range of materials and properties [30]:

- Band Structure and DOS: WIEN2k provides accurate band structures and density of states, which are essential for understanding electronic properties.
- Optical Properties: It can calculate optical spectra, including dielectric functions and absorption coefficients.
- Magnetic Properties: WIEN2k supports spin-polarized calculations, making it suitable for studying magnetic materials.
- Structural Optimization: The software can optimize crystal structures by minimizing the total energy with respect to atomic positions and lattice parameters.
- Surface and Defect Studies: WIEN2k can model surfaces, interfaces, and defects in materials, providing insights into their electronic and structural behavior[16].

I-6-4 Advantages and Limitations

- Advantages:
    - High accuracy due to the full-potential approach.

- Suitable for a wide range of materials, including metals, semiconductors, insulators, and strongly correlated systems.
- Extensive documentation and a large user community for support.

- Limitations:
  - Computationally demanding, especially for large systems or high-precision calculations.
  - Requires careful selection of parameters, such as MT radii and linearization energies.
  - Limited to periodic systems, making it less suitable for isolated molecules or disordered systems.

I-6-5 Initialization:

It constructs by the spatial configuration (geometry), symmetry operations, starting densities, the number of special points necessary for integration in the irreducible Brillouin zone…etc. All these operations are carried out thanks to a series of small auxiliary programs that generate:

- NN: This program uses the case.struct file in which the atomic positions in the unit cell are specified, calculates the nearest neighbor distances for all atoms, and checks that the corresponding atomic spheres (radii) do not overlap [38].
- LSTART: this program generates atomic densities and determines how the different orbitals are treated in the band structure calculation, such as core states with or without local orbitals.
- SYMMETRY: it allows the generation of atomic densities and determines how the different orbitals are treated in the band structure calculation, such as core states with or without local orbitals.
- KGEN: generates a mesh of k points in the Brillouin zone
- DSTART: generates a starting density for the SCF cycle by superimposing the atomic densities gen

SCF Calculation the SCF cycle includes the following steps:

- LAPW0: generates the potential from the density.
- LAPW1: calculates the valence bands (the eigenvalues and the eigenvectors)
- LAPW2: calculates the valence densities from the eigenvectors.
- LCORE: calculates heart states and densities.
- MIXER: Mixes the input and output densities [17].

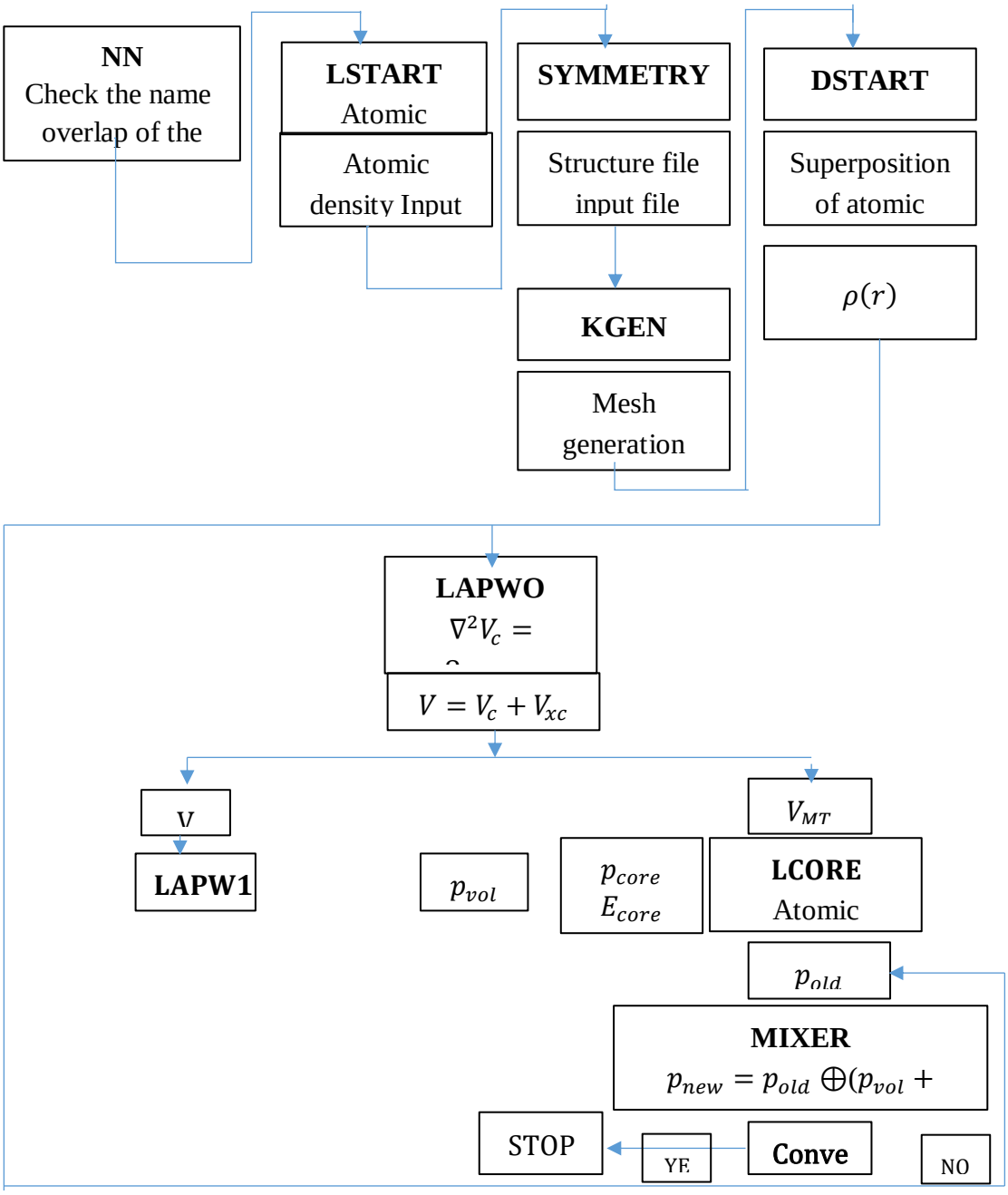

Figure I.4: algorithm of code win2k

I-7 Conclusion

The Win2K program utilizes Density Functional Theory (DFT) to solve the Schrödinger equation for many-electron systems, providing an efficient and accurate approach to studying electronic structures. DFT simplifies the complexity of the many-body Schrödinger equation by focusing on electron density rather than individual wavefunctions, making it computationally feasible for large systems like molecules and solids. Win2K implements the Kohn-Sham equations, which approximate the behavior of interacting electrons using a system of non-interacting particles in an effective potential. This allows the program to calculate key properties such as band structures, density of states, total energies, and atomic forces. By leveraging exchange-correlation functionals like LDA or GGA, Win2K delivers reliable results for a wide range of materials, including metals, semiconductors, and insulators. Its versatility and efficiency make it a powerful tool for exploring electronic, magnetic, and optical properties, as well as for predicting material behavior in various applications.

References

[1] M. A. Pena and J. L. G. Fierro, "Chemical structures and performance of perovskite oxides," Chem. Rev., vol. 101, no. 7, pp. 1981–2018, 2001.

[2] E. Schrödinger, "An Undulatory Theory of the Mechanics of Atoms and Molecules," Phys. Rev., vol. 28, no. 6, pp. 1049–1070, 1926.

[3] D. J. Griffiths, *Introduction to Quantum Mechanics*, 2nd ed., Pearson Prentice Hall, 2005.

[4] R. Shankar, *Principles of Quantum Mechanics*, 2nd ed., Springer, 1994.

[5] D. R. Hartree, "The wave mechanics of an atom with a non-Coulomb central field. Part I: Theory and methods," Math. Proc. Camb. Phil. Soc., vol. 24, pp. 89–110, 1928.

[6] M. Levy, "Electron densities in search of Hamiltonians," Phys. Rev. A, vol. 26, no. 3, pp. 1200–1208, 1982.

[7] D. R. Hartree and V. Fock, "The Self-Consistent Field with Exchange for Atoms," Z. Phys., vol. 61, no. 1–2, pp. 126–148, 1930.

[9] A. Szabo and N. S. Ostlund, *Modern Quantum Chemistry: Introduction to Advanced Electronic Structure Theory*, Dover, 1996.

[10] W. Kohn and L. J. Sham, "Self-Consistent Equations Including Exchange and Correlation Effects," Phys. Rev., vol. 140, no. 4A, pp. A1133–A1138, 1965.

[11] R. M. Martin, *Electronic Structure: Basic Theory and Practical Methods*, Cambridge University Press, 2004.

[12] P. Hohenberg and W. Kohn, "Inhomogeneous Electron Gas," Phys. Rev., vol. 136, no. 3B, pp. B864–B871, 1964.

[13] J. P. Perdew and K. Burke, "Comparison of the generalized gradient approximation and the Hartree-Fock method," Int. J. Quantum Chem., vol. 57, no. 3, pp. 309–319, 1996.

[14] R. G. Parr and W. Yang, *Density-Functional Theory of Atoms and Molecules*, Oxford University Press, 1989.

[15] M. E. Casida, "Time-dependent density functional response theory for molecules," in *Recent Advances in Density Functional Methods*, World Scientific, 1995, pp. 155–192.

[16] J. Hafner, "Ab-initio simulations of materials using VASP: Density-functional theory and beyond," J. Comput. Chem., vol. 29, no. 13, pp. 2044–2078, 2008.

[17] M. Born and J. R. Oppenheimer, "On the quantum theory of molecules," Ann. Phys., vol. 389, no. 20, pp. 457–484, 1927.

[18] J. P. Perdew and A. Zunger, "Self-interaction correction to density-functional approximations for many-electron systems," Phys. Rev. B, vol. 23, no. 10, pp. 5048–5079, 1981.

[19] J. P. Perdew et al., "Atoms, molecules, solids, and surfaces: Applications of the generalized gradient approximation for exchange and correlation," Phys. Rev. B, vol. 46, no. 11, pp. 6671–6687, 1992.

[20] Y. Zhang and W. Yang, "Comment on 'Generalized Gradient Approximation Made Simple'," Phys. Rev. Lett., vol. 80, no. 4, pp. 890–890, 1998.

[21] J. Heyd, G. E. Scuseria, and M. Ernzerhof, "Hybrid functionals based on a screened Coulomb potential," J. Chem. Phys., vol. 118, no. 18, pp. 8207–8215, 2003.

[22] A. D. Becke, "Density-functional thermochemistry. III. The role of exact exchange," J. Chem. Phys., vol. 98, no. 7, pp. 5648–5652, 1993.

[23] J. C. Slater, "Wave functions in a periodic potential," Phys. Rev., vol. 51, no. 10, pp. 846–851, 1937.

[24] O. K. Andersen, "Linear methods in band theory," Phys. Rev. B, vol. 12, no. 8, pp. 3060–3083, 1975.

[25] B. Segall, "The muffin-tin approximation," Solid State Phys., vol. 20, pp. 1–152, 1967.

[26] D. J. Singh and L. Nordström, *Planewaves, Pseudopotentials and the LAPW Method*, Springer, 2006.

[27] P. Blaha, K. Schwarz, G. Madsen, D. Kvasnicka, and J. Luitz, *WIEN2k, An Augmented Plane Wave + Local Orbitals Program for Calculating Crystal Properties*, Vienna University of Technology, 2001.

[28] K. Schwarz and P. Blaha, "Solid state calculations using WIEN2k," Comput. Mater. Sci., vol. 28, no. 2, pp. 259–273, 2003.

[29] G. K. H. Madsen et al., "BoltzTraP. A code for calculating band-structure dependent quantities," Comput. Phys. Commun., vol. 175, no. 1, pp. 67–71, 2006.

[30] L. D. Marks, "WIEN2k made easy," Comput. Phys. Commun., vol. 182, no. 9, pp. 1861–1865, 2011.

[33] P. Blaha et al., "WIEN2k: An APW+lo program for calculating the properties of solids," J. Chem. Phys., vol. 152, no. 7, 074101, 2020.

[38] WIEN2k User's Guide, P. Blaha et al., Vienna University of Technology, 2020.

Chapter 2: Results and Discussion

II.1. Introduction

This chapter is dedicated to the theoretical study of the structural, electronic, magnetic, and optical properties of the $AgMnS_2$ compound. Based on the ab initio calculation methods described in the previous chapter, particularly the Density Functional Theory (DFT) implemented in the WIEN2k code, we aim to explore the fundamental characteristics of this material. The objective is to provide a detailed understanding of its behavior, starting with the determination of its crystal structure and structural parameters, then examining its electronic, magnetic, and optical properties, relying on the provided calculation results.

Delafossite-structured oxides, with the general formula AMO_2, represent a fascinating class of materials that have garnered significant interest due to their unique structural, electronic, and optical properties. Named after the French mineralogist Gabriel Delafosse, these compounds were first discovered in 1873 by Charles Friedel in a Siberian graphite sample. The Delafossite structure consists of alternating layers of monovalent cations ($A^+ = Cu^+, Ag^+, Pd^+, Pt^+$) in linear coordination and trivalent transition metals (M^{3+}) in edge-sharing octahedral coordination. This arrangement leads to a variety of polytypes, primarily the rhombohedral (3R) and hexagonal (2H) phases, distinguished by their oxygen stacking sequences.

Over the years, research on Delafossites has evolved from fundamental crystallographic studies to explorations of their potential applications in transparent conductive oxides, thermoelectric materials, and photocatalysis. The stability of the Delafossite phase is highly dependent on ionic radii and coordination preferences, with the A^+ cation playing a crucial role in structural integrity. Additionally, the distortion of the $[MO_6]$ octahedron and the variation in lattice parameters (a, c) with cation size further influence the material's properties.

This report provides an overview of the historical background, structural characteristics, stability factors, and polytypism in Delafossite compounds, with a particular focus on copper-based Delafossites ($CuMO_2$). Understanding these aspects is essential for tailoring Delafossite materials for advanced technological applications.

I-2 History

In 1873, Charles Friedel first reported the existence of a mixed oxide of copper and iron, $CuFeO_2$ during the observation of a graphite sample from Siberia [1].This mineral was named Delafossite in honor of French mineralogist and crystallographer Gabriel Delafosse (1795-1878).Later, the Rogers' work confirmed the existence of this mineral in a number of mines of copper in the United States [2,3].The crystalline structure of Delafossite, with the formula ABO_2, was established in 1935 by Soller and Thompson on a synthetic sample [4] and then confirmed by Pabst on a natural sample [5].

Delafossite-structured oxides represent an interesting family of materials relatively little studied during the 20th century despite the interest both fundamental and applied that they can represent.In 1971, Shannon, Prewitt, and Rogers published three major articles on the synthesis, crystal structure, and electrical properties of several Delafossite-structured compounds ($PtCoO_2$, $PdCoO_2$, $CuFeO_2$, and $AgFeO_2$) [6-8].It was only in 1997 that the interest of scientists in the interest of scientists in these Delafossite-structured compounds exploded, following the work of Kawazoe and al [9].

I-3 Chemical Formula and Stability of the Delafossite Phase

Chemical Formula

Delafossites are compounds of the type AMO_2 where A is a monovalent element that adopts a linear (II) coordination (A = Ag, Cu, Pd, or Pt) and the cation M can be composed of most trivalent transition metals, group III elements, rare earths, or charge-compensated pairs (for example M^{2+} / M^{4+}).A particularity of this structure is that the ionic radius of the trivalent element M, which is stabilized in octahedral (VI) coordination, can vary widely from that of aluminum (rAl^{3+} = 0.535 Å) to that of lanthanum (rLa^{3+} = 1.032 Å), according to Shannon's effective ionic radii table [10], which leads to a significant increase in the unit cell volume.The different AMO_2 compounds with Delafossite structure are represented in FIGURE(II-1).Based on the ratio of ionic radii $r(A^{+}$ II)/$r(M^{+3}$ VI), Beznosikov et al. [11] even predicted the existence of other Delafossite-structured compounds that have not yet been developed.

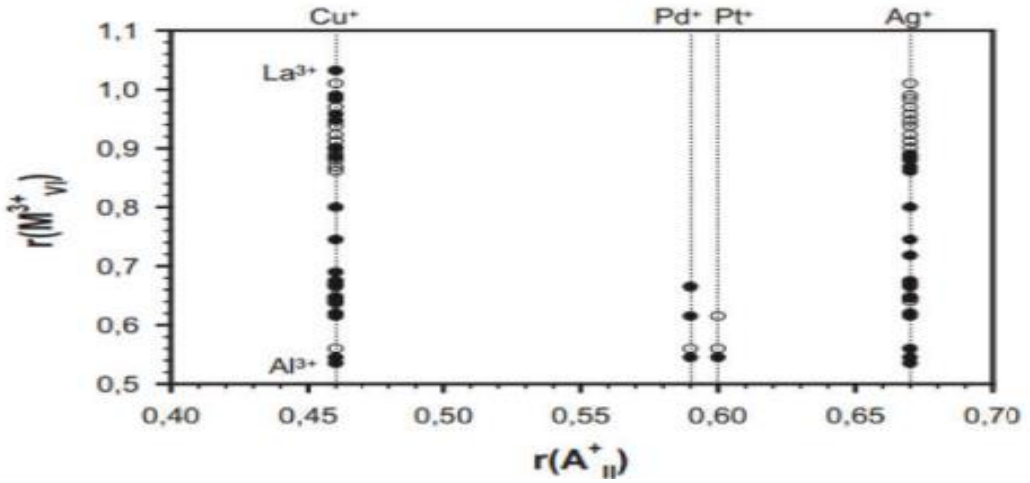

FIGURE(II-1): volume.The different AMO_2 compounds with Delafossite structure.

I.4. Stability of the Delafossite phase

Ternary oxides with the chemical formula AMO_2 can form a variety of structural phases.The advantage of forming one phase over another depends on several factors.The most important factor is the coordination of the cations A and M.Four individual coordination classes of AMO_2 compounds have been identified [12].

They are given in TABLE II-1 with an example of a compound for each structure.3^+These classes are relatively determined by the diameters of the A^+ and M^{3+} cations.Small cations simply cannot withstand significant coordination due to the oxygen crowding that would result, while large cations would require higher coordination numbers.By combining all the ionic radius information for AMO_2 compounds, a structure field map can be drawn as shown in FIGURE(II-2)

TABLE II-1: The coordination classes of AMO_2-type compounds.

Classe de coordination	Composés typique	Symétrie
$A^{VI}B^{VI}O_2{}^{VI}$	NaCl	Cubique
	α-NaCl	Rhomboédrique
	α-$LiFeO_2$	Tétragonal
$A^{IV}B^{IV}O_2{}^{IV}$	β-$NaFeO_2$	Orthorhombique
$A^{VIII}B^{IV}O_2{}^{VI}$	$KFeO_2$	Orthorhombique
$A^{II}B^{VI}O_2{}^{IV}$	$CuFeO_2$ Delafossite	Rhomboédrique
	$CuYO_2$ Delafossite	Hexagonal

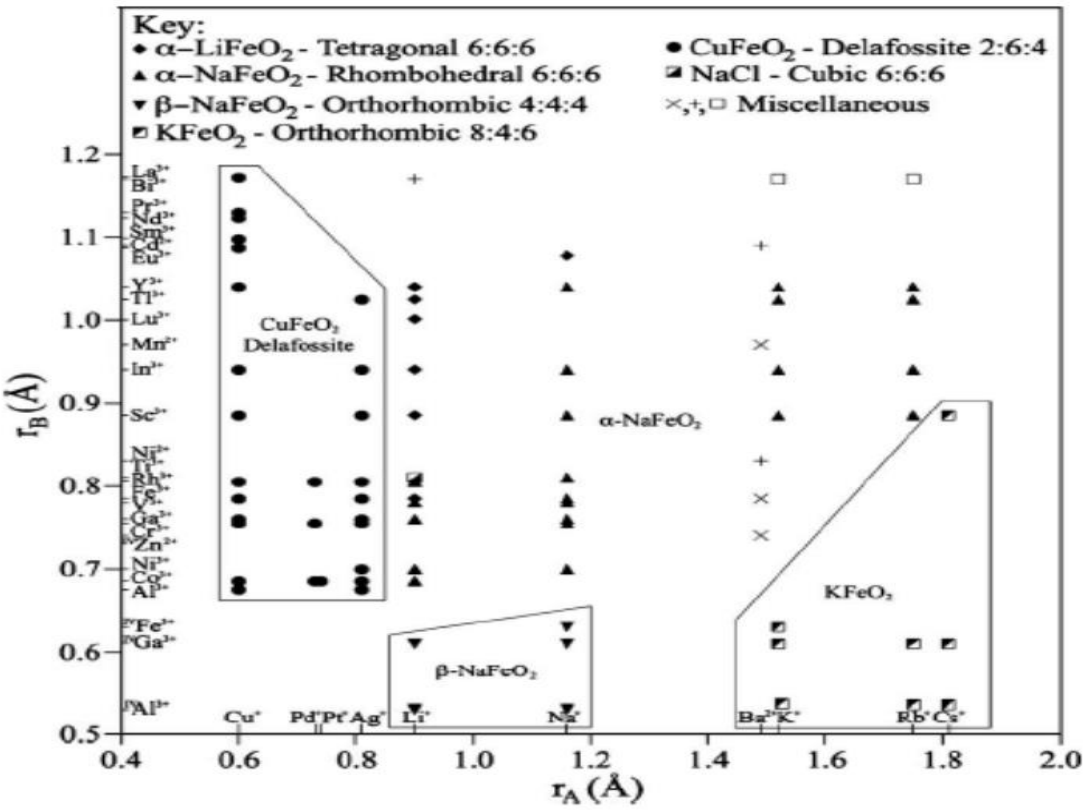

FIGURE(II-2): Structural field map of the AM(B)O_2 compounds[12].

Delafossites with the formula $A^+M^{3+}O_2$ and a coordination scheme of 2:6:4 have a constitution that is both limited (for A^+) and largely open (for M^{3+}).These compounds consist of cation A with the smallest ionic radius of all AMO_2-type oxides [12].As seen inFIGURE(II-1), the Delafossite structure is stable for only four ions at the A site (Cu^+, Ag^+, Pd^+, and Pt^+), while several M cations are possible.Even when the Delafossite phase can form for a given A-M cation combination, its formation depends on various factors.Structural factors that have already been discussed regarding the radius of the cations and the coordination environment

I-5 Structural Properties of Delafossites

I-5-1 Description of the Delafossite structure

The Delafossite structure AMO_2 can be visualized as consisting of two alternating layers: a planar layer of A cations in a triangular pattern and a layer of MO_6 octahedra, interconnected by their edges, flattened along the c-axis FIGURE(II-3.a) .

Thus, this structure is composed of double layers of compact stacking of oxygen atoms whose octahedral sites are occupied by M^{3+} ions and whose internal cohesion (between layers) is ensured by A^+ ions.The latter are linearly associated with two oxygens belonging to the MO_6 octahedral layers of two consecutive layers, upper and lower, to form AO^{23-} groups.Each A^+ ion has six close A^+ neighbors in the plane parallel to that of the double layers of oxygen.The oxygen ion is in pseudo-tetrahedral coordination with one A cation and three FIGURE(II-3.b).

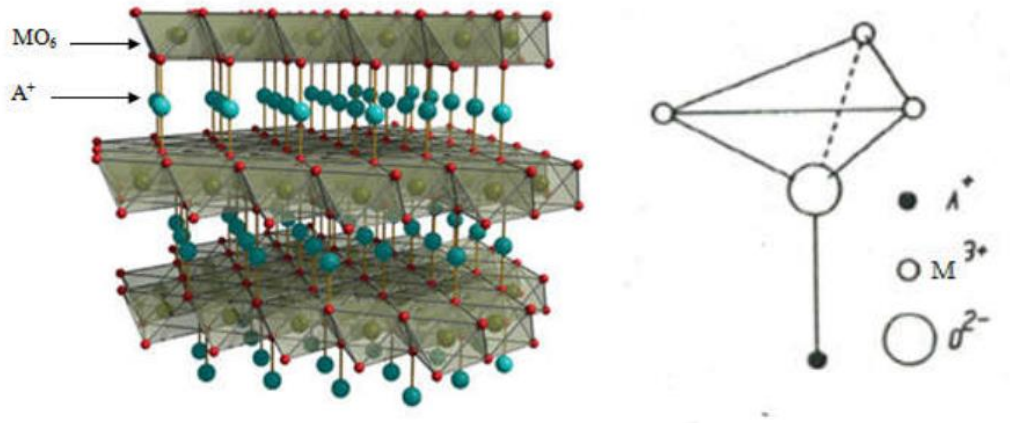

FIGURE(II-3): (a) Representation of the Delafossite-type structure.(b) Coordination polyhedron of oxygen.

I-5-2 Distortion of the octahedron [MO_6]

In the Delafossite structure, although the 6 M-O distances are equal, the [MO_6] octahedron is slightly flattened along the third-order axis parallel to c (rhombic symmetry D3d).The degree of distortion of the octahedron is therefore evaluated through the ratio (dO-Oi)/(dO-Oiv), with dO-Oi being the length of the edge of an octahedron parallel to the base plane of the hexagonal lattice, and dO-Oiv being the length of the edge joining two oxygens on either side of the M^{3+} ion layer (schematized in the inset of FIGURE(II-4)).The evolution of the distortion of the MO_6 octahedron as a function of the radius of the M^{3+} ion is illustrated in FIGURE(II-4).[13].

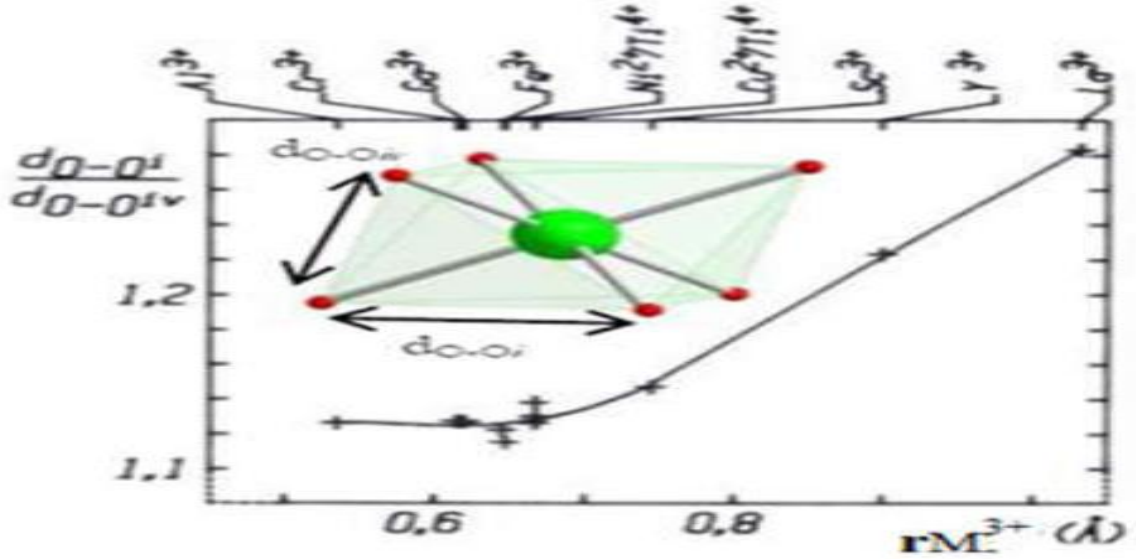

FIGURE(II-4): Variation with the radius of the M^{3+} ion of the distortion of the MO_6 octahedron [13].

It can be observed in this figure that the ratio (d O-Oi)/(d O-Oiv) increases with the radius of the M^{3+} ion.The importance of the distortion of the D3d symmetry of the octahedron can actually be simply correlated with the evolution of the covalence of the M-O bonds.It should be taken into consideration that:

The M-O bond is all the more covalent as the contribution of the 2p orbitals of oxygen to this bond is more significant (the 2p orbitals are less stable due to the 2s orbital).

The angle M-O-M is smaller the less flattened the MO_6 octahedron is and that the ratio (dO-Oi)/(d O-Oiv) approaches unity.

All these considerations of the bonds show that when the size of M decreases and consequently the strength of the M-O bonds increases, one can reasonably expect that the angle M-O-M will decrease as well as the ratio (d O-Oi)/(d O-Oiv).

I-5-3 Polytypes of the Delafossite structure

Such an atomic arrangement in this type of structure can easily give rise to various polytypes according to the different sequences of close packing that can be envisaged for the oxygen layers.

if we call O_1, O_2, and O_3 the three possible types of oxygen planes, we can observe, for example, sequences:

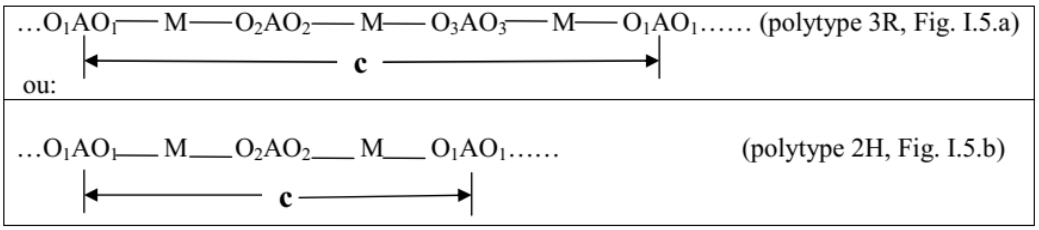

which correspond, respectively, to a rhombohedral polytype (3R) of space groups R-3m and a hexagonal polytype (2H) of space groups P63/mmc. The difference between the two polytypes lies in the third layer.

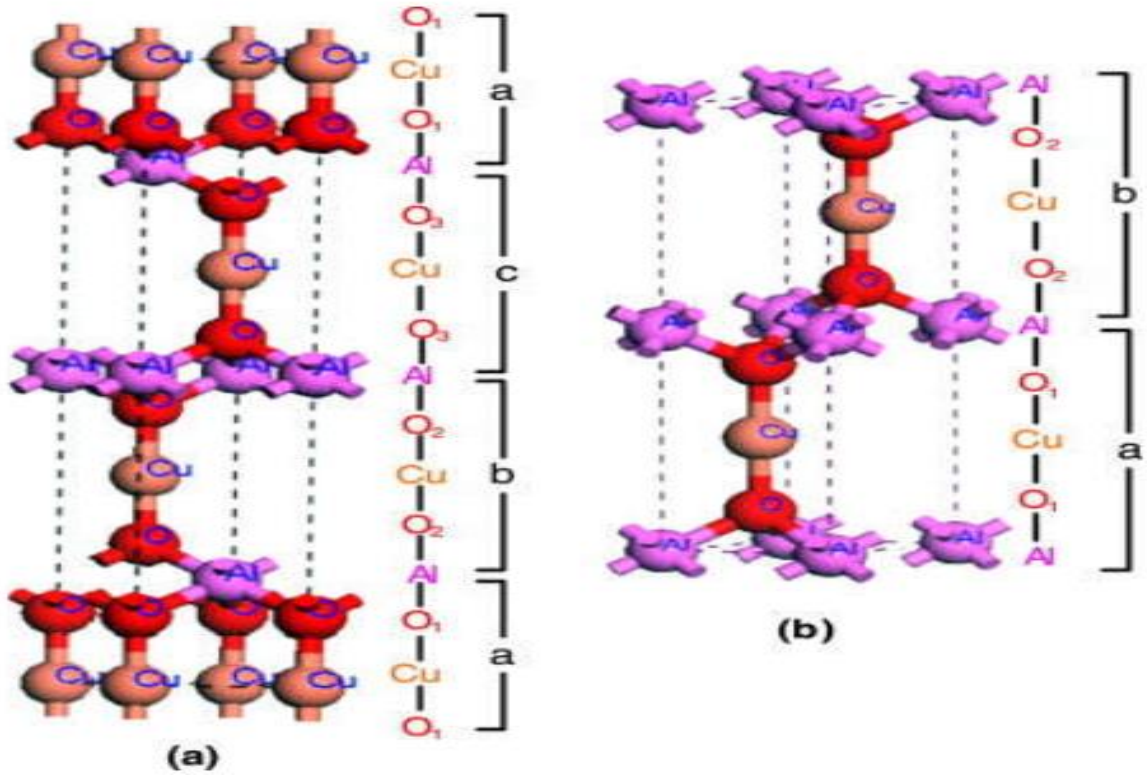

FIGURE(II-5): Representation of compact stacking sequences in the polytypes: (a) 3R and (b) 2H of the compound $CuAlO_2$.

In fact, the main difference between the 2H and 3R polytypes lies in the orientation of the successive layers [MO_6].The 2H Delafossite has its octahedral layers rotated 180° relative to each other and consequently, the structure is described with two basic blocks: A-B and B-A(FIGURE(II-6).a and b) [14].

Whereas in 3R Delafossite, these layers have the same orientation and the structure is described with three blocks: A-B, B-C, and C-A (FIGURE(II-6).c and d) [14], where the letters A to C indicate the three usual triangular positions in a compact oxygen stacking.

Due to this difference in stacking, a transformation of the 2H structure into 3R is not possible through a topotactic process and requires breaking the M-O bonds.

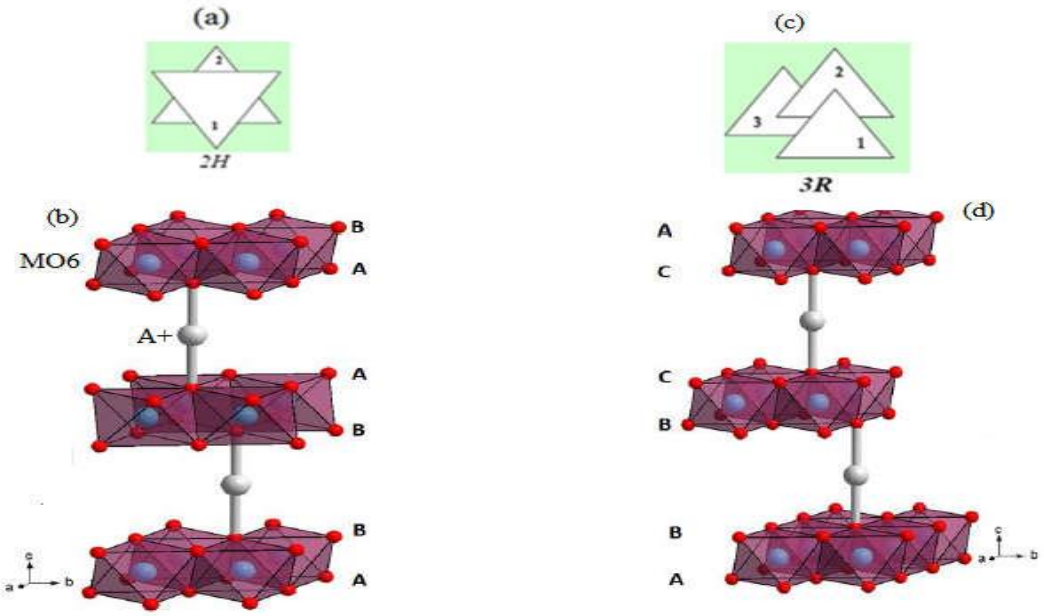

FIGURE(II-6): Schematic representations of the arrangement of octahedra in (a) 2H and (c) 3R.Representations of the oxygen stacking sequences in (b) 2H and (d) 3R

FIGURE(II-7)(a-f) show representations of the two polytypes of the Delafossite structure.FIGURE(II-7). b and e respectively provide a projection onto the (110) plane of the two polytypes 2H and 3R.

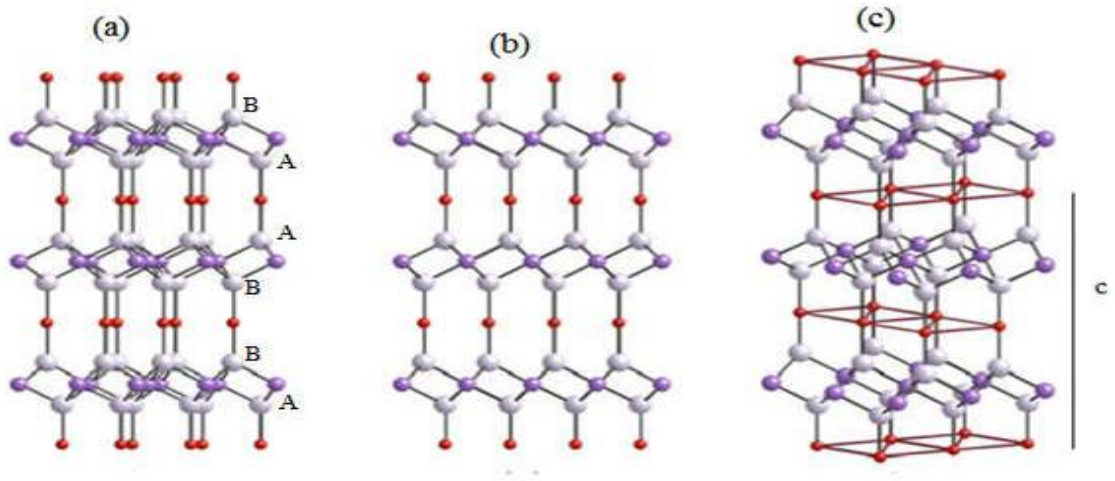

FIGURE(II-7): The structure of Delafossite.(a) 2H polytype; (b) Projection of 2H polytype on the (110) plane; (c) Stacking of the two layers in 2H.(d) 3R polytype; (e) Projection of 3R polytype on the (110) plane; (c) Stacking of the three layers in 3R [12].

I-5-4 The unit cell

The unit cells of the two polytypes, 2H and 3R, are respectively represented in FIGURE(II-8.a) and b.Note that the value of the lattice parameter a in both polytypes is ≈ 3Å, whereas the value of c is ≈ 17Å for the 3R polytype and 11Å for the 2H polytype FIGURE(II-8.c)

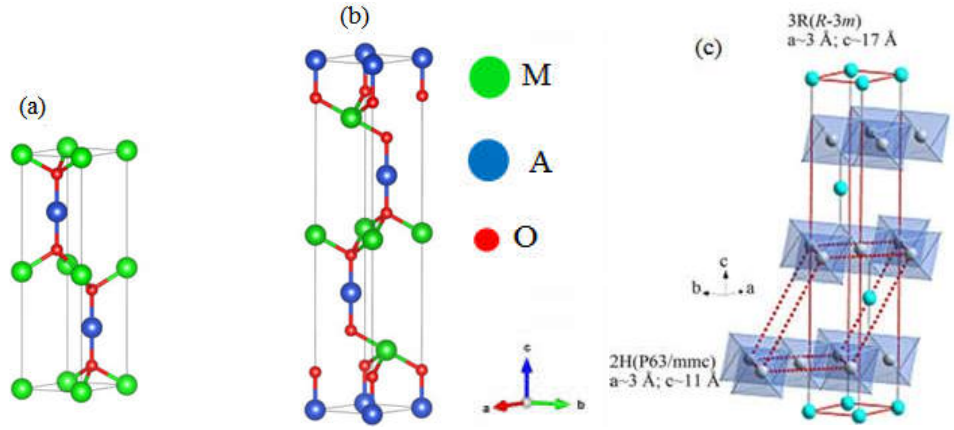

FIGURE(II-8): Representations of the elementary cells of the polytypes (a) 2H, (b) 3R, and (c) 2H and 3R [24].

It should be noted that the most frequently encountered polytype is 3R, and only a few Delafossites, where M belongs to group IB, exhibit the 2H polytype such as $CuAlO_2$, $CuScO_2$, or $CuYO_2$ [15].It should also be noted that a study [17] conducted on $CuMO_2$-type

Delafossites, where M is taken from two different groups, IIIA and IIIB, revealed that Delafossites from the IIIA and IIIB groups stabilize respectively in rhombohedral and hexagonal structures.

A 6H polytype has also been reported for the Delafossites $AgFeO_2$, $AgCoO_2$, and $AgCrO_2$ [16], which combines the two polytypes 3R and 2H.

I-5-5 Lattice Parameter

The lattice parameters in Delafossite can be correlated with the sizes of the cations A and M, which influence the O-A-O, M-O, A-A, or M-M distances [19].In the Delafossite, all O-A-O bonds are strictly parallel to the c-axis, and it is expected that the value of the a parameter varies according to the A-A or M-M interaction.Experimentally, it appears that the lattice parameter along the a-axis preferentially depends on the M cations FIGURE(II-9).This is mainly attributed to the larger size of the M cations compared to the A cations, leading to a higher M-M repulsion and thus an increase in the lattice parameters along the a-axis.Furthermore, the +III charge on M compared to the +I charge on A also influenced the stronger M-M repulsion [18].Moreover, the lattice parameter a is equal to the length of the edges of the octahedra [MO_6].

It is therefore directly correlated to the radius of the cation M.The lattice parameter along the c-axis is largely determined by the length of the O-A-O bond.Due to the repulsive nature of M^{3+} cations along the shared octahedral edges, a distortion occurs, resulting in a shortening of the interatomic distances between the oxygen anions.When the radius of the cation M increases, the M-O distance increases while the O-O contact distance remains relatively unchanged.Therefore, an increase in the size of the cations M has little impact on the c lattice parameter FIGURE(II-9) .

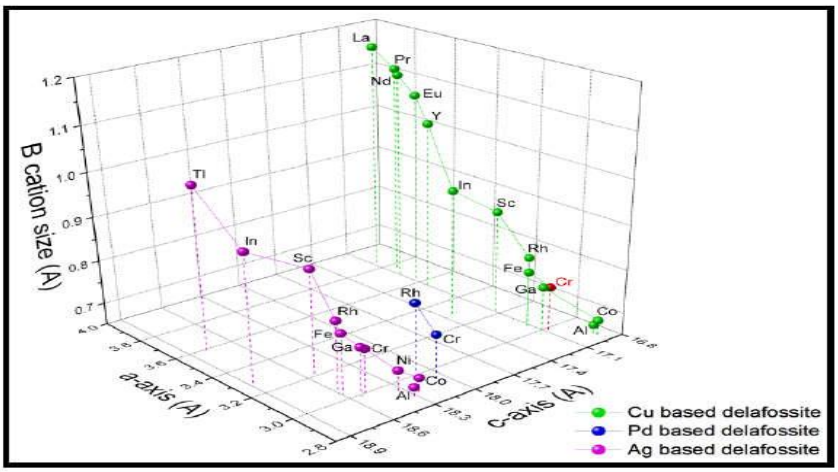

FIGURE(II-9): Influence of cations M on the lattice parameters a and c of Delafossite [19].

IV. The family of copper Delafossite

Regarding Delafossite-type oxides $A^{+}M^{3+}O_2$ with the Cu+ ion in the "A" site, there are currently many compounds that contain a wide variety of elements on the "M" site, ranging from small cations with an ionic radius between 0.54-0.67Å to large lanthanide cations (0.95Å-1.16Å).

In this series of compounds, as observed in FIGURE(II-10) , the value of the lattice parameter "a" increases when the size of the M^{3+} cation grows, while the "c" parameter remains almost unchanged.

TABLE II-2: summarizes the structural data of some compounds$CuMO_2$, $CuMII0.5M'IV0.5O_2$, and $CuMII1/3M'III1/3M'IV1/3O_2$ with Delafossite structure known.

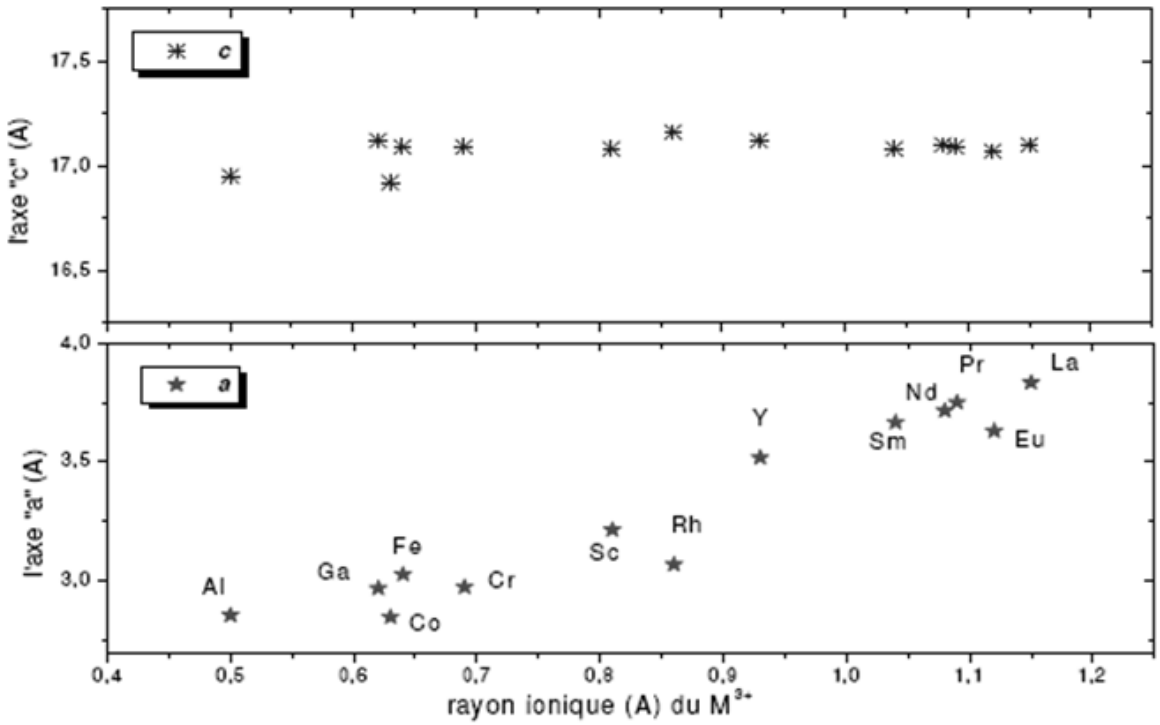

FIGURE(II-10): The variation of lattice parameters as a function of the ionic radius values of M^{3+} for the $Cu^{+}M^{3+}O_2$ compounds .

TABLE II-2: Structural data of $CuMO_2$ Delafossite compounds .

Composé	*r(M_{VI}^{3+}) (Å)*	*Polytype*	*a (Å)*	*c (Å)*
$CuAlO_2$	0,535	3R	2,8571	16,940
		2H	2,8630	11,314
$CuCoO_2$	0,610	3R	2,8488	16,920
$CuCrO_2$	0,615	3R	2,9750	17,096
$CuGaO_2$	0,620	3R	2,9750	17,154
$CuFeO_2$	0,645	3R	3,0351	17,166
$CuRhO_2$	0,665	3R	3,0740	17,094
$CuScO_2$	0,745	3R	3,2204	17,100
		2H	3,2230	11,413
$CuInO_2$	0,800	3R	3,2922	17,338
$CuYO_2$	0,900	3R	3,5330	17,136
		2H	3,5310	11,418
$CuEuO_2$	0,947	3R	3,6300	17,080
$CuSmO_2$	0,958	3R	3,6500	17,030
$CuNdO_2$	0,983	3R	3,7100	17,090
$CuPrO_2$	0,990	3R	3,7500	17,050
$CuLaO_2$	1,032	3R	3,8300	17,100
$CuCo_{0,5}Ti_{0,5}O_2$	0,675	3R	3,0330	17,183
		2H	3,0177	11,449
$CuCu_{0,5}Ti_{0,5}O_2$	0,668	3R	3,0350	17,163
		2H	3,0400	11,460
$CuNi_{0,5}Sn_{0,5}O_2$	0,690	3R	3,0090	17,240
$CuNi_{0,5}Ti_{0,5}O_2$	0,648	3R	3,1170	17,329
$CuNi_{1/3}V_{2/3}O_2$	0,637	3R	2,9865	17,191

Conclusion:

Delafossite oxides (AMO_2) exhibit a rich structural chemistry governed by the interplay of ionic radii, coordination environments, and stacking sequences. The 3R and 2H polytypes, arising from different oxygen layer arrangements, demonstrate how subtle variations in atomic positioning can lead to distinct crystallographic phases. The distortion of the [MO_6] octahedron, influenced by the M^{3+} cation size, further highlights the delicate balance between ionic and covalent bonding in these materials.

Copper-based Delafossites ($CuMO_2$) are particularly noteworthy due to their tunable electronic properties, making them promising candidates for transparent electronics, thermoelectrics, and optoelectronic devices. The nearly constant c-axis parameter (despite changes in M^{3+} size) and the increasing a-axis parameter with larger M^{3+} cations underscore the structural adaptability of Delafossites.

Future research should focus on synthesizing new Delafossite variants, exploring their electronic and magnetic properties, and optimizing their performance in functional applications. Advances in computational modeling and experimental techniques will further enhance our understanding of these materials, paving the way for innovative uses in energy conversion, catalysis, and beyond.

II.1. Computational Details:

The calculations of the properties of the $AgMnS_2$ compound are assumed to be performed using the Full-Potential Linearized Augmented Plane Wave (FP-LAPW) method within the framework of Density Functional Theory (DFT), as implemented in the WIEN2k code. Approximations for the exchange-correlation potential, such as the Generalized Gradient Approximation (GGA) under the PBE (Perdew-Burke-Ernzerhof) or PBEsol parameterization, as well as more advanced approaches like the modified Becke-Johnson potential (mBJ) for optoelectronic properties, would typically be employed. Calculation parameters such as the number of k-points in the irreducible Brillouin zone, the RMT*Kmax parameter determining the plane wave basis set size, and the muffin-tin radii (RMT) for each atom type (Ag, Mn, S) should be carefully chosen to ensure calculation convergence.

[Note: These details are based on common practices and the methodology of the original chapter. Specific details for the $AgMnS_2$ calculations were not initially available, but the graphical results suggest the use of these methods.]

II.2. Structural Properties

II.2.1. Crystal Structure of the $AgMnS_2$ Compound:

Preliminary analysis based on the available results indicates that the $AgMnS_2$ compound crystallizes in a Tetragonal schematically illustrates this crystal structure.

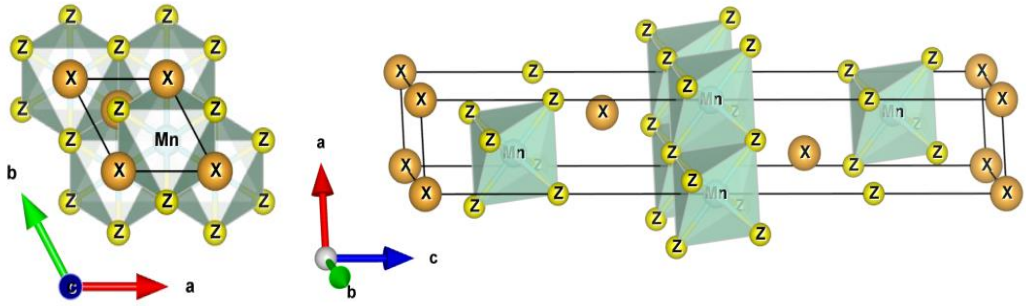

FIGURE(II-11): Schematic representation of the Tetragonal crystal structure of the $AgMnS_2$ compound.

TABLE II-3:. The calculatedatomic positions using PBE-Sol approximations of $AgMnS_2$ compound.

		GGA			Autres travaux		
Materials	**Atoms**	**x**	**y**	**z**	**x**	**y**	**z**
AgMnS2	Ag	0,0000	0,0000	0,0000	0,0000	0,0000	0,0000
	Mn	0,5000	0,5000	0,5000	0,0000	0,0000	0,5000
(R-3/m # 166)	S	0,7701	0,77010	0,7701	0,0000	0,0000	0,2508
	S	0,2298	0,2298	0,2298	0,0000	0,0000	0,2508

TABLE II-3: The calculated equilibrium lattice constants, bulk modulus, and cohesive energy for compound obtained by using PBE-SOL approximations.

		a (Å)	c(Å)	B(GPa)	Ecoh(eV/atom)
AgMnS2	GGA	3.3463	14,3311	184,9220	5.22
	Theo	3,0014	14,558	-	-

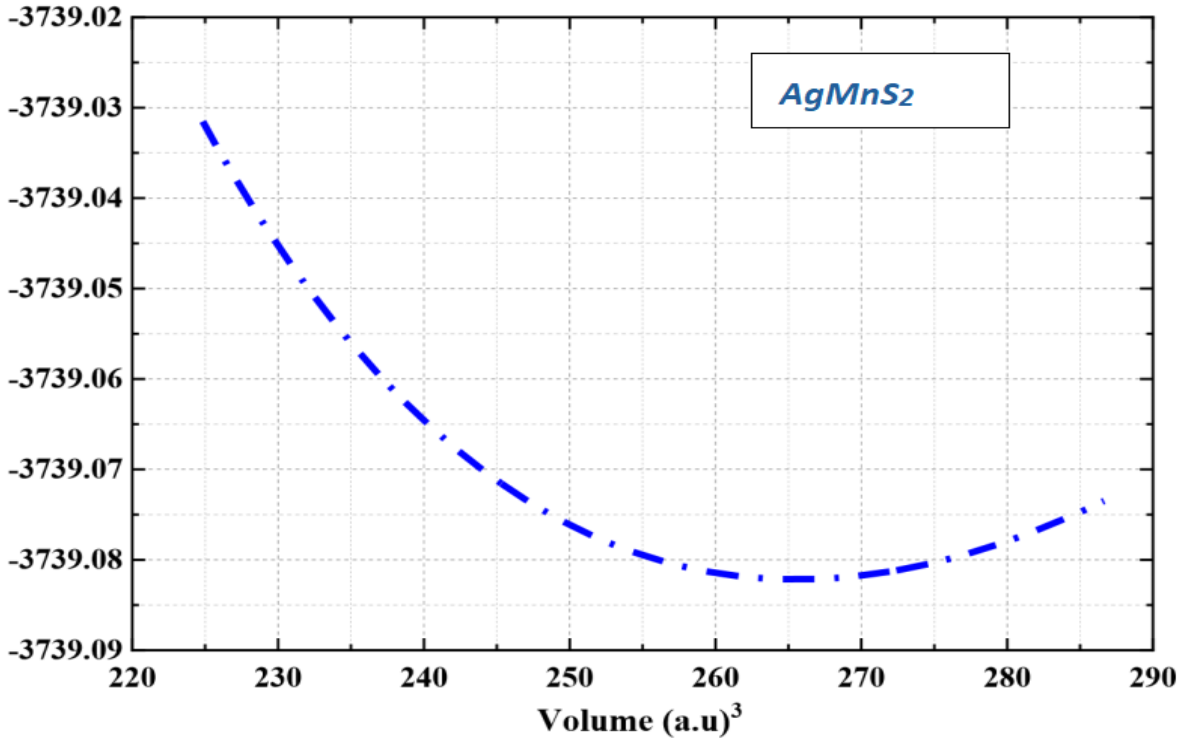

FIGURE(II-12).Variation de l'énergie totale en fonction du volume.

En ce qui concerne l'énergie de cohésion de la molécule, elle a été calculée à l'aide de la formule suivante : **(II.4)**

$$E_{cohésion} = \frac{\left(E_{atom}^{Ag} + E_{atom}^{Mn} + 2 \times E_{atom}^{S}\right) - E_{tot}^{AgMnS2}}{N_{Ag} + N_{Mn} + N_{S2}}$$

Où E_{tot}^{AgMnS2} est l'énergie totale à l'équilibre. E_{atom}^{Ag} E_{atom}^{Mn} , E_{atom}^{S2} sont les énergies atomiques

des atomes de Ag, Mn et S respectivement.N_{Ag}, N_{Mn} , N_S Sont les nombres d'atomes dans la maille unitaire du composé $AgMnS_2$

Selon les valeurs de l'énergie de cohésion et le module de compressibilité obtenus en utilisant deux approximations, On peut dire que ce composé a une bonne rigidité, c'est-à-dire qu'il résiste à la déformation contre la compression. On peut également remarquer que ce composé à une plus grande énergie de cohésion à l'état ferromagnétique qu'à l'état paramagnétique, ce qui confirme sa stabilité à l'état ferromagnétique.

More detailed information regarding the lattice parameters (a, c), the exact atomic positions within the unit cell, and the specific space group of this tetragonal structure for $AgMnS_2$ are not available from the provided data.

II.3.2. Ground State of $AgMnS_2$

Determining the ground state would normally involve calculating the total energy of the $AgMnS_2$ compound as a function of the unit cell volume for different possible structural or magnetic configurations (e.g., ferromagnetic, antiferromagnetic, paramagnetic). Fitting the energy-volume curve to an equation of state, such as the Birch-Murnaghan equation, would allow the determination of equilibrium parameters: the equilibrium volume (V_0), the bulk modulus (B_0), and its first pressure derivative (B'). The cohesive energy could also be calculated to assess the thermodynamic stability of the compound.

The data in FIGURE(II-12) show the variation of the magnetic moment as a function of volume, suggesting that calculations were performed for different volumes, but the

corresponding energy data are not available to determine the ground state and equilibrium structural parameters.

III.1.The origin of magnetism

In this part we studied the magnetic properties of the compound, and before that we will recall the origin of magnetism in materials [7–12], and this at three levels:

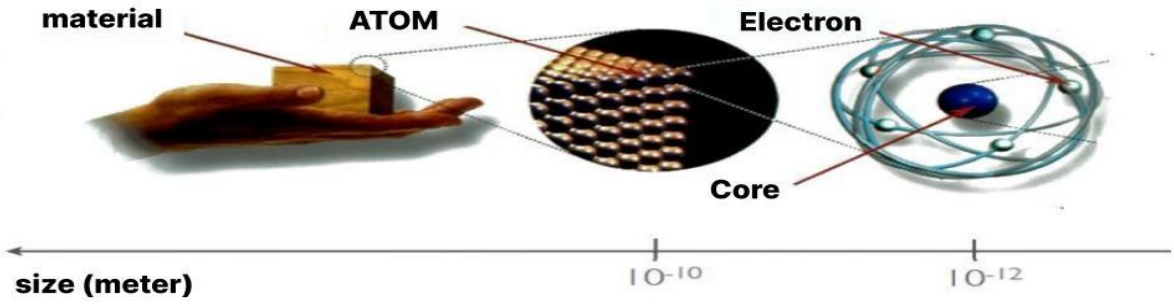

FIGURE(II-13). The origin of magnetism of materials.

III.2.At the electron level :

as we know, each electric charge is in motion, it generates a magnetic field, and since the electron is a particle in motion around itself and around the nucleus , these two movements will generate two magnetic moments:

a) A magnetic moment of spin $\vec{\mu}s = -g \frac{\mu B}{h} \vec{S}$ where g is the Landé parameter and $\hbar$ is the Planck constant.

b) An orbital magnetic moment $\vec{\mu}sI = \frac{\mu B}{h} \vec{I}$ where μ_B is the Bohr magneton.

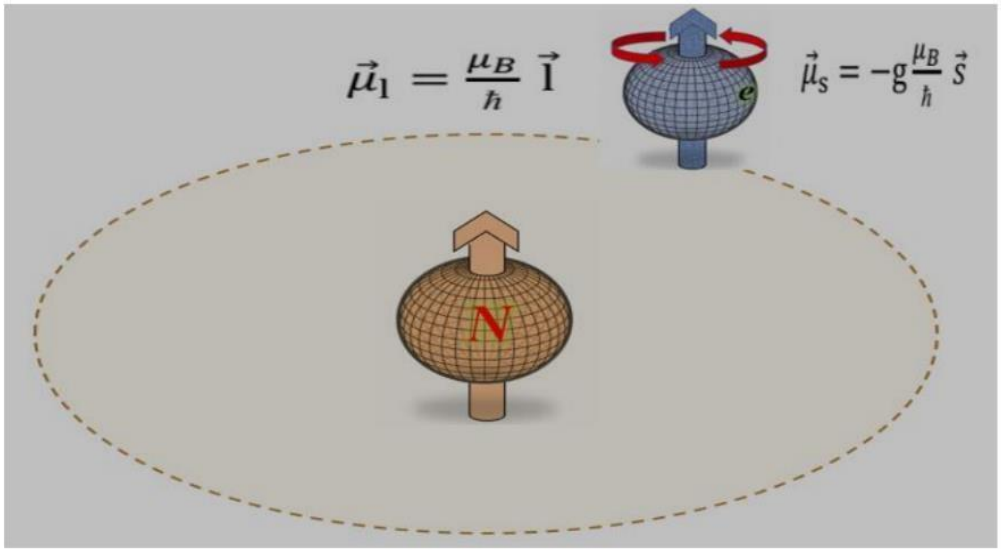

FIGURE(II-14). The origin of magnetism at the electron level

III.3.At the level of the atom :

The magnetism of the atom is linked to the electrons in its outer shell; if all electrons are placed in the outer layer in a paired manner, the sum of the magnetic moments of these two electrons is zero and therefore the atom is non-magnetic, and vice versa.

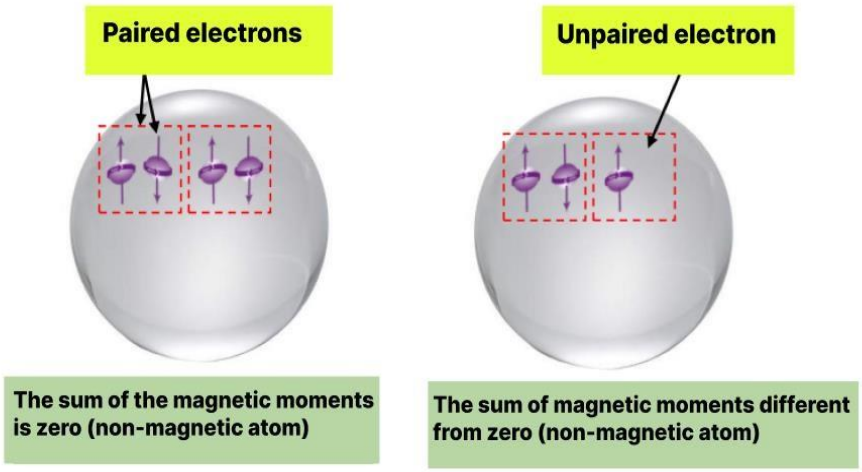

FIGURE(II-15). the origin of magnetism at the atom level.

III.4.At the level of material :

The magnetic state of matter depends on the nature of the atoms making up the matter (magnetic or not), the distances between the atoms and the exchange interactions between them, the effect of temperature and the applied magnetic field. Regarding the magnetic interactions between atoms, they are quantum exchange interactions related to the magnetic moments of the atoms, the distance between them, and the external magnetic field that they are subject to. These interactions were described by the Heisenberg Hamiltonians given by:

$$H_{mag} = \sum_{ij} j_{ij} \vec{S}_j \vec{S}_{ij} + \sum_i g_i \mu_B \vec{h} \vec{S}_i \qquad \textbf{(II.4)}$$

Where μ_B is the Bohr magneton, g_i is the magnetic ratio, $\vec{S}_i$ is a spin operator, $\vec{h}$ is the external magnetic field, and J_{ij} is the exchange coupling constant (it depends

on the distance between the two atoms). The different states of the magnetic moments of the atoms whose exchange interaction is shown in FIGURE(II-16) .

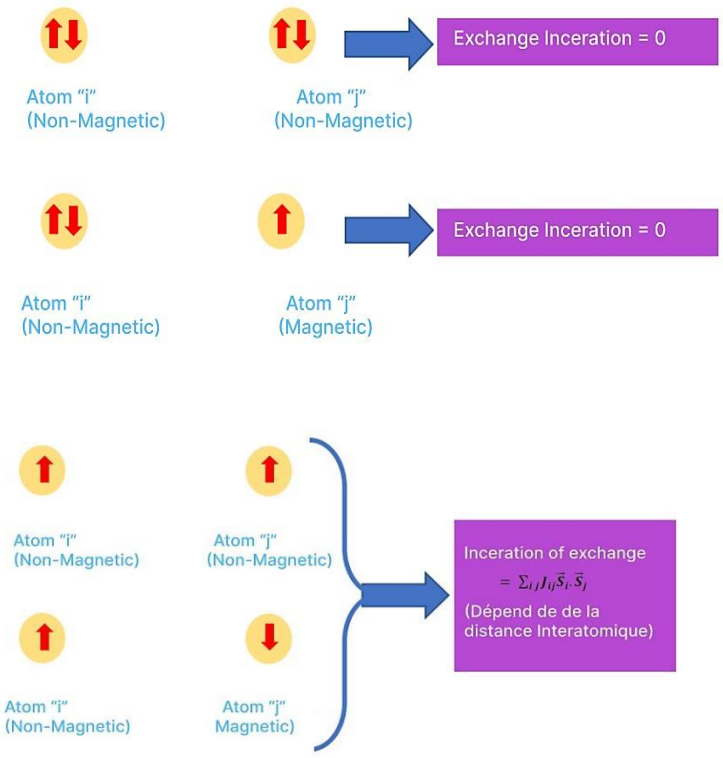

FIGURE(II-16). The origin of magnetism at the level of matter (the different cases of exchange interaction between the magnetic moments of atoms.

Depending on the nature of the atoms making up matter and the alignment of the magnetic moments, we distinguish five types of magnetism:

A) Diamagnetism:

The magnetic material [7–12] consists of non-magnetic atoms, because all its electrons are paired, which means that the total magnetic moment of the atoms is zero.

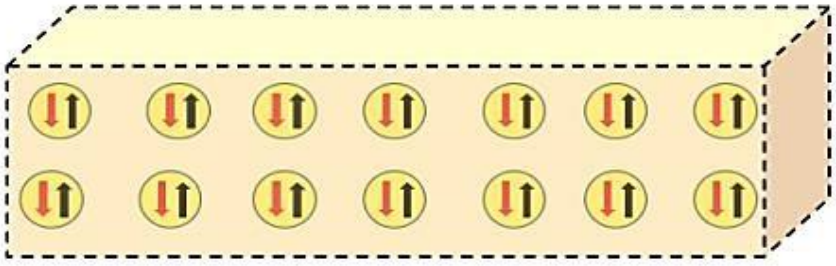

FIGURE(II-17.a).lustration of atoms in a state Diamagnetism

B) Paramagnetism:

The atoms of the paramagnetic material contain unpaired electrons, and therefore these atoms have magnetic moments without any exchange interactions between them due to the large distance between them. Therefore its magnetic moments are randomly directed so that the sum of the total torque of the material is equal to zero[7–12].

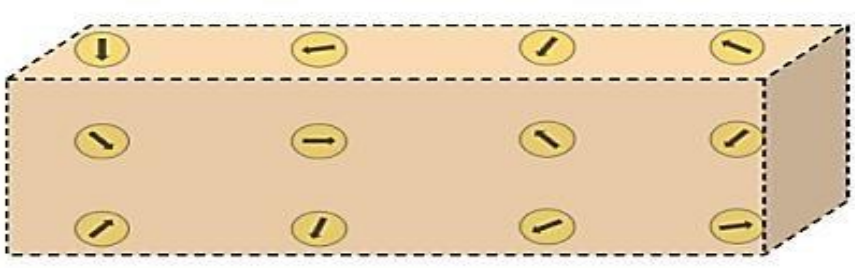

FIGURE(II-17.b). lustration of atoms in a state Paramagnetism.

C) Ferromagnetism:

The atoms of the ferromagnetic material are composed of unpaired electrons, an exchange interaction occurs between them due to the small distance between them, so that the exchange integral J_{ij} is negative, so the electrons line up in parallel[7–12].

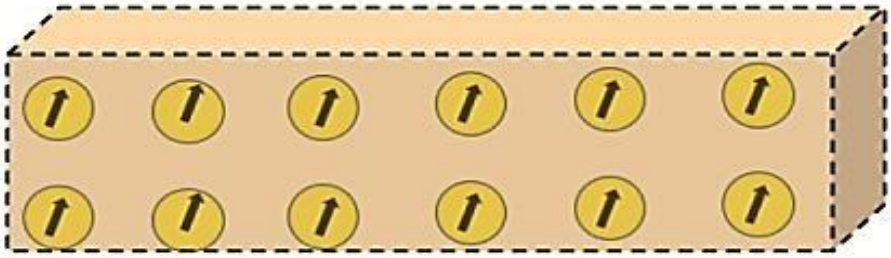

FIGURE(II-17.c). lustration of atoms in a state Ferromagnetism.

D) Antiferromagnetism:

exchange interaction occurs between them due to the small distance is small enough, so the exchange coupling constant J_{ij} is positive , so the electrons align themselves antiparallel, then the atoms are organized in such a way that two neighboring atoms can have opposite magnetic moments and consequently the net moment of the material is zero[7–12].

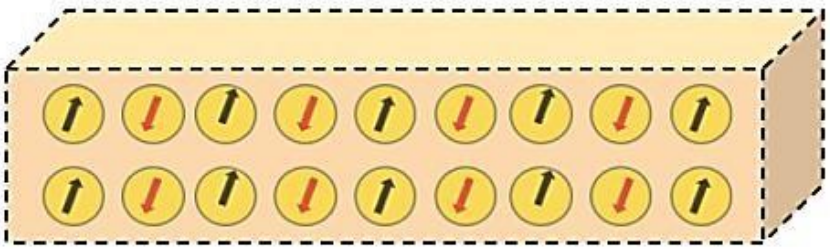

FIGURE(II-17.d). lustration of atoms in a state Antiferromagnetism.

E) Ferrimagnetism:

This is a similar state to the antiferromagnetic case, except that the magnetic moments that are arranged antiparallel are not equal, and therefore, the material has a magnetic moment which is not zero [7–12].

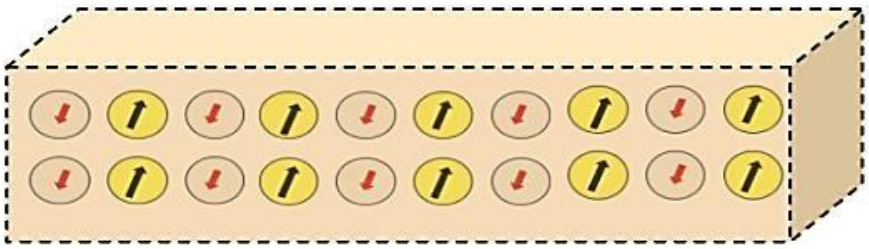

FIGURE(II-17.e).lustration of atoms in a state Ferrimagnetism.

III.5.Variation of the magnetic moment under the effect of pressure:

Using the GGA approximation, we were able to calculate the total moment of the maille unitaire as well as the contribution of each atome to this moment. The obtained results, which are shown in Table II.3, indicate that the compound $BrCdO_2$ exhibits ferromagnetic behavior with a total magnetic moment of 3.

It is also observed that the predominant magnetic contributors at this time are the bromum atomes, with the remaining atomes contributing almost nothing.

The variation in the maille's volume can have an impact on the total magnetic moment. As we can see in the magnetic moment increases as the bulk volume of the compound decreases.

The study of magnetic properties is crucial, especially for compounds containing transition elements like Manganese (Mn).FIGURE(II-18) presents the results of the calculation of the total magnetic moment (TOT) and partial moments (for Ag, Mn, S, and the interstitial region INT) as a function of the unit cell volume.

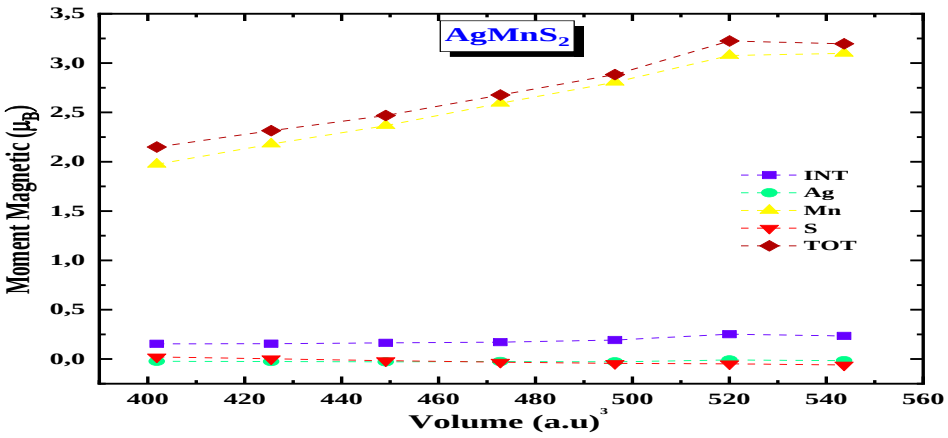

FIGURE(II-18): Variation of total and partial magnetic moments as a function of volume for $AgMnS_2$.

Analysis of FIGURE(II-18) reveals several important points:

• Volume Dependence: The total magnetic moment (TOT) shows a strong dependence on volume, increasing significantly with lattice expansion. It rises from approximately 2.15 μB at 400 a.u.³ to a maximum of about 3.2 μB at 520 a.u.³, before decreasing slightly. This dependence suggests a sensitivity of magnetic exchange interactions to interatomic distances.

• Origin of Magnetism: The main contribution to the magnetic moment clearly comes from the Manganese (Mn) atoms. The local magnetic moment on Mn closely follows the trend of the total moment, increasing from ~2.0 μB to ~3.1 μB over the studied volume range. This is expected for a 3d transition ion like Mn.

• Minor Contributions: The contributions from Ag and S atoms are negligible, remaining close to zero across the entire volume range. The interstitial region (INT) exhibits a small but noticeable polarized magnetic moment (~0.15 to 0.25 μB) that also slightly increases with volume.

• Nature of Magnetic Order: The presence of a significant net magnetic moment, primarily due to Mn, indicates a magnetically ordered state, likely ferromagnetic or ferrimagnetic in nature, although the exact configuration cannot be determined without additional information (e.g., energy comparison of FM and AFM states).

These results highlight the dominant role of Mn d-electrons in the magnetism of $AgMnS_2$ and the strong influence of the crystal volume on the magnitude of this magnetism.

IV.1.Electronic Properties

The analysis of electronic properties relies mainly on the calculation of the band structure and the density of states (DOS), presented in Figures II.3 and II.4, respectively.

IV.1.1. Band Structure

FIGURE(II-19) shows the calculated band structure for $AgMnS_2$ for both spin channels(Spin Up and Spin Down).

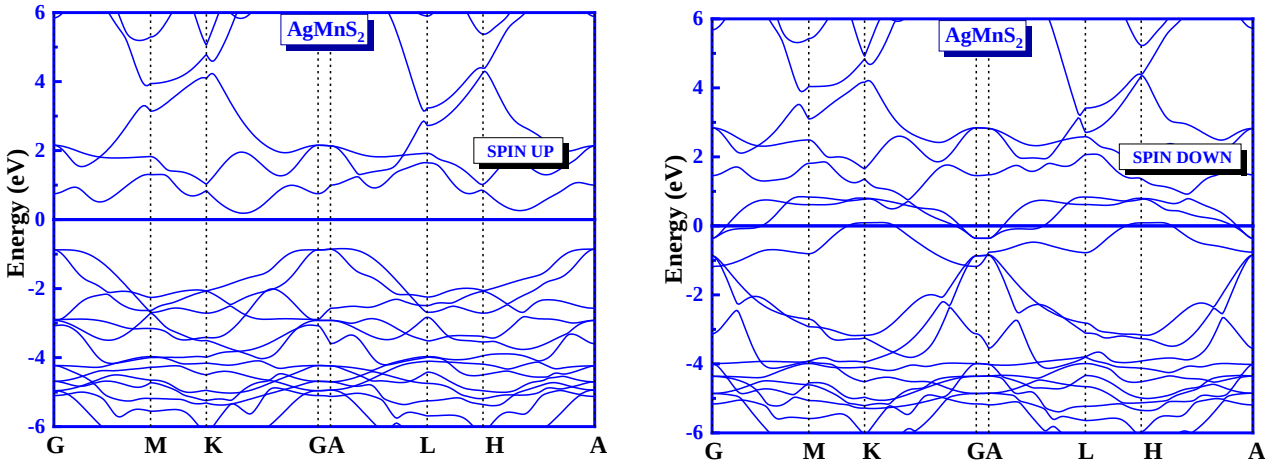

FIGURE(II-19): Band structure of $AgMnS_2$ along high symmetry directions for Spin Up (top) and Spin Down (bottom) channels. The Fermi level is at 0 eV.

The analysis of the band structure reveals distinct behavior for each spin channel:

• Spin Up Channel (Top): Several bands cross the Fermi level (0 eV). There is no energy gap. This clearly indicates metallic behavior for the Spin Up channel.

• Spin Down Channel (Bottom): The Valence Band Maximum (VBM) and the Conduction Band Minimum (CBM) are both located at the G (Γ) high symmetry point. The VBM is slightly below

0 eV (~ -0.2 eV) and the CBM is significantly above (~ +1.8 eV). This indicates a direct gap of approximately 2.0 eV. This behavior is characteristic of a semiconductor for the Spin Down channel.

The combination of metallic behavior in one spin channel and semiconducting behavior in the other spin channel gives the $AgMnS_2$ compound a Half-metallic nature. This property is highly sought after for spintronics applications, as it theoretically allows for a fully spin-polarized electron current at the Fermi level.

IV.2. Electronic Density of States

FIGURE(II-20) presents the total density of states (TDOS) and partial density of states (PDOS) projected onto the atomic orbitals (s, p, d) of each element (Ag, Mn, S).

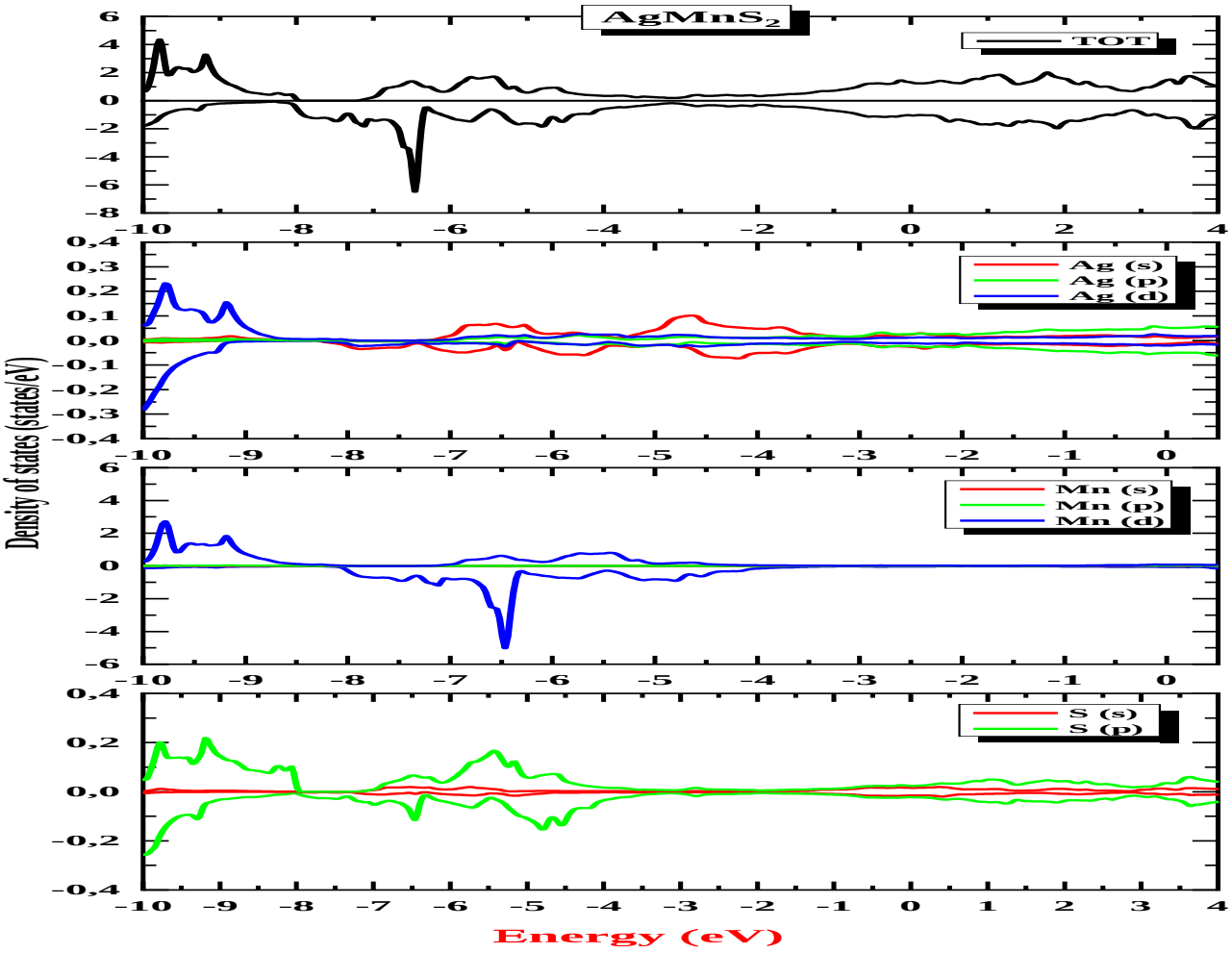

F

IGURE(II-20): Total (TDOS, top) and partial (PDOS) density of states for

Ag, Mn, and S in $AgMnS_2$. Spin Up is positive, Spin Down is negative. The Fermi level is at 0 eV.

The DOS analysis corroborates and details the observations made from the band structure:

• TDOS: The TDOS confirms the asymmetry between the Spin Up and Spin Down channels, characteristic of a magnetic material. It shows a finite density of states at the Fermi level (0 eV) for the Spin Up channel (positive) and an absence of states (gap) around the Fermi level for the Spin Down channel (negative), confirming the half-metallic nature.

• PDOS - Manganese (Mn): Mn-d states dominate the density of states near the Fermi level. The significant energy shift (exchange splitting) between the Spin Up and Spin Down Mn-d states is the primary source of the large observed magnetic moment. Mn-d Spin Up states contribute significantly to the density at the Fermi level, explaining the metallic character of this channel.

• PDOS - Sulfur (S): S-p states are predominant in the valence band, between -6 eV and -2 eV. There is notable hybridization between S-p and Mn-d states in this region, indicating significant Mn-S covalent bonding that influences the electronic structure.

• PDOS - Silver (Ag): Ag-d states are localized at lower energies within the valence band (mainly between -6 eV and -3 eV). Their contribution near the Fermi level is minimal.

In summary, the DOS confirms the half-metallic nature of $AgMnS_2$, highlights the crucial role of Mn-d states in magnetism and conduction in the Spin Up channel, and illustrates the Mn-d / S-p hybridization in chemical bonding.

channel. However, the metallic character of the Spin Up channel complicates the overall optical analysis and could lead to high reflectivity in certain energy ranges.

A detailed study would require the explicit calculation of optical spectra (e.g., absorption coefficient, refractive index), which are not available in the provided data.

IV.2. Conclusion

This chapter presented a theoretical study of the structural, magnetic, and electronic properties of the $AgMnS_2$ compound based on DFT calculation results provided graphically. The analysis revealed that $AgMnS_2$ crystallizes in a Tetragonal structure and exhibits strong magnetic properties dominated by Mn atoms, with a total magnetic moment strongly dependent on volume. The study of the electronic structure (bands and DOS) highlighted a remarkable feature: $AgMnS_2$ is a half-metal, behaving as a metal for Spin Up electrons and as a semiconductor with a direct gap of approximately 2.0 eV for Spin Down electrons. This property, combined with intrinsic magnetism, makes $AgMnS_2$ potentially interesting for spintronics applications. Mn-d states play a predominant role in these properties, with significant hybridization with S-p states. Additional information would be needed to determine the exact equilibrium structural parameters and to analyze the optical properties in detail.

References - Chapter II

[1] C. Friedel, 'Sur un oxyde de cuivre et de fer', Comptes Rendus, vol. 76, p. 1154, 1873.

[2] A. F. Rogers, 'Notes on American occurrences of Delafossite', Am. Mineral., vol. 1, pp. 129–131, 1916.

[3] A. F. Rogers, 'Delafossite from Colorado', Am. Mineral., vol. 2, pp. 76–78, 1917.

[4] K. Soller and A. R. Thompson, 'X-ray study of Delafossite', Phys. Rev., vol. 48, no. 1, pp. 49–52, 1935.

[5] A. Pabst, 'Natural Delafossite from Nevada', Am. Mineral., vol. 25, pp. 75–80, 1940.

[6] R. D. Shannon, C. T. Prewitt, and A. F. Rogers, 'Chemistry of noble metal oxides', Inorg. Chem., vol. 10, no. 4, pp. 713–718, 1971.

[7] J. M. D. Coey, *Magnetism and Magnetic Materials*, Cambridge University Press, 2010.

[8] S. Blundell, *Magnetism in Condensed Matter*, Oxford University Press, 2001.

[9] H. Kawazoe et al., 'P-type electrical conduction in transparent thin films of CuAlO2', Nature, vol. 389, pp. 939–942, 1997.

[10] R. D. Shannon, 'Revised effective ionic radii and systematic studies of interatomic distances in halides and chalcogenides', Acta Crystallogr. A, vol. 32, no. 5, pp. 751–767, 1976.

[11] A. G. Beznosikov and V. A. Belov, 'Structure field of layered oxides of the Delafossite type', Kristallografiya, vol. 41, pp. 991–997, 1996.

[12] M. Preiser, C. A. Kuntscher, F. Lichtenberg, and A. Loidl, 'Delafossite-type oxides: structure and properties', Phys. Rev. B, vol. 70, no. 16, 165109, 2004.

[13] C. Wolverton and A. Zunger, 'Electronic structure and stability of Delafossite oxides', Phys. Rev. B, vol. 52, pp. 8813–8822, 1995.

[14] T. Okuda et al., 'Structure and transport properties of CuCrO2', J. Solid State Chem., vol. 153, no. 2, pp. 317–321, 2000.

[15] K. Ueda, H. Hosono, and H. Kawazoe, 'Synthesis of new p-type Delafossite oxides', Appl. Phys. Lett., vol. 70, no. 25, pp. 3561–3563, 1997.

[16] J. Tate et al., 'Structural polytypes in layered oxides: 2H and 3R Delafossites', J. Solid State Chem., vol. 146, pp. 555–561, 1999.

[17] T. Ohta and H. Hosono, 'Electronic structure and phase stability of CuMO2', J. Appl. Phys., vol. 90, no. 7, pp. 3296–3300, 2001.

[18] H. J. Kim et al., 'Lattice parameter trends in Delafossite oxides', J. Mater. Sci., vol. 42, no. 22, pp. 9374–9381, 2007.

[19] K. Momma and F. Izumi, 'VESTA: A three-dimensional visualization system for electronic and structural analysis', J. Appl. Crystallogr., vol. 44, pp. 1272–1276, 2011.

[24] D. J. Singh, 'Electronic structure calculations with the LAPW method', Springer, 2006.

General Conclusion

Delafossite is considered a material with a promising future, and research is ongoing to explore its applications across various sectors. Here, we present some of the challenges currently facing research as a prelude to future studies. From the perspective of synthesis and processing, these materials should feature low-cost manufacturing methods. They also pose a significant challenge in terms of their functions and applications in sensor devices, due to their specific advantages in this field.

The goal we aimed to achieve through this work is to study and investigate the structural, electronic, and magnetic properties of the compound $AgMnS_2$, which is considered one of the most important and widely used compounds in many fields. The aim is to determine the most suitable domain for utilizing the $AgMnS_2$ compound, in addition to understanding the role and type of each atom that influences a particular property.

This objective was achieved using the WIEN2k simulation software within the framework of Density Functional Theory (DFT), based on the Full-Potential Linearized Augmented Plane Wave (FP-LAPW) method, in order to solve the Schrödinger equation for a crystalline system containing a large number of interacting atoms and electrons. To achieve this, we introduced several simplifications, such as the Born-Oppenheimer approximation, as well as other approximations like Hartree, Hartree-Fock, and DFT.

Finally, by evaluating, classifying, and discussing the potential opportunities in chalcogenides, this study aims to encourage further research into this growing class of semiconductors, thereby enabling future advancements in optoelectronic devices and supporting new approaches in the development of thin-film photovoltaic technologies in the years to come.

Résumé

Dans ce travail, nous avons étudié les propriétés structurelles, électroniques et magnétiques du composé $AgMnS_2$ en utilisant la méthode des ondes planes augmentées linéarisées (FP-LAPW) basée sur la théorie de la fonctionnelle la densité (DFT). Pour estimer le terme d'échange-corrélation, nous avons utilisé l'approximation GGA. Dans les propriétés structurelles, nous avons calculé les paramètres de la maille, le module de compressibilité et l'énergie de cohésion. Pour comprendre le comportement électronique du composé, nous avons analysé la structure des bandes électronique les spectres de la densité d'états électroniques. Nous avons également étudié la distribution de la densité de charge dans la région interatomique pour connaitre la nature de la liaison entre les atomes. Nous avons calculé le moment magnétique total et partiel du composé.

Abstract

In this work, we studied the structural, electronic and magnetic properties of the compound $AgMnS_2$ using the linearized augmented plane wave (FP LAPW) method based on density functional theory (DFT). To estimate the exchange-correlation term, we used the GGA approximation. In the structural properties, we calculated the mesh parameters, the compressibility modulus and the cohesion energy. To understand the electronic behavior of the compound, we analyzed the structure of the electronic bands and the spectra of the density of electronic states. We also studied the distribution of the charge density in the inter-atomic region to know the nature of the bond between the atoms. We calculated the total and partial magnetic moment of the compound.

ملخص

في هذا العمل، قمنا بدراسة الخصائص التركيبية والإلكترونية والمغناطيسية لمركب AgMnS2 باستخدام طريقة الموجة المستوية الخطية المعززة FP-LAPW(المعتمدة على نظرية الكثافة الوظيفية) DFT(. لتقدير مصطلح ارتباط التبادل، استخدمنا تقريب GGA. في الخواص الهيكلية، قمنا بحساب معلمات الشبكة ومعامل الانضغاطية وطاقة التماسك. لفهم السلوك الإلكتروني للمركب، قمنا بتحليل بنية النطاقات الإلكترونية وأطياف كثافة الحالات الإلكترونية. كما قمنا بدراسة توزيع كثافة الشحنة في المنطقة بين الذرات لمعرفة طبيعة الرابطة بين الذرات. قمنا بحساب العزم المغناطيسي الكلي والجزئي للمركب.